Noname manuscript No.
(will be inserted by the editor)

Subharmonic resonance and critical eccentricity for the classical hydrogen atomic system

Daniel C. Cole

Received: date / Accepted: date

Abstract Previous research investigated the subharmonic resonant behavior for the classical hydrogen atom, with classical radiation damping and circularly polarized light acting on the classical electron. The predicted behavior is believed to be physically accurate when the electron lies far from the nucleus, so that quantum mechanical effects are minimized, thereby applying to Rydberg atomic situations and highly excited hydrogen states. This work examines several new physical effects. First, the semimajor axis is shown to remain relatively constant when in subharmonic resonance; second, the eccentricity steadily increases until a maximum value is reached, at which point orbital decay again sets in. If the initial orbit is circular, the maximum value of the eccentricity, ε, before decay sets in, is shown to always be the same value for each subharmonic condition. Specifically, with f_1 being the applied frequency of light and with $n = 2, 3, 4, ...$, denoting the subharmonic orbital frequency corresponding to $\frac{1}{n} \times f_1$, then a unique and critical value of ε occurs for each n before decay sets in, where $\varepsilon_2 < \varepsilon_3 < \varepsilon_4 < ...$, regardless of the initial radius of the circular orbit. A mixture of simulation results are shown, combined with an analytic derivation for these critical values of eccentricity.

Keywords hydrogen · Rydberg · stochastic electrodynamics · simulation · classical · nonlinear · subharmonic · resonance

Mathematics Subject Classification (2000) 70Kxx · 65Pxx · 65Zxx

1 Introduction

The present article builds on work first discussed in [1]; related work can be found in [2],[3],[4],[5],[6]. The Rydberg atom is considered here again, with the key example being of a hydrogen atom in a high excited state, so that classical physics can safely

Daniel C. Cole
Dept. of Mechanical Engineering, 110 Cummington Mall, Boston University, Boston, MA 02215.
Tel.: +617-353-0432
E-mail: dccole@bu.edu

be applied in the main analysis. Reference [1] showed that when a circularly polarized (CP) plane wave is directed normal to the outer electron's orbit, strong subharmonic resonances occur that prevent orbital decay for surprisingly long times, and under a fairly wide range of conditions. As shown, if the electric field amplitude of the CP light exceeds a certain value that depends to first degree on the order of the subharmonic resonance, but also on the semimajor axis value and relative phase, then orbital and energy decay can be held at bay for times long compared to the classical time of orbital decay. This system is taken up here again, but new results and a deeper analysis and understanding are provided.

By subharmonic resonance, we mean here the behavior of the classical electron's orbit when the period of the orbit is equal to an integer multiple of $n = 2, 3, 4, 5, ...,$ etc., times the period of the incident CP plane wave; or, in other words, the orbital frequency of the classical electron orbit is equal to $\frac{1}{2}$, $\frac{1}{3}$, $\frac{1}{4}$, etc., to that of the frequency of the incident plane wave. Here we will show that when the classical electron is caught in one of these subharmonic resonances, starting initially in a circular orbit, then the semimajor axis, a, remains fairly constant, with a relatively small fluctuation that grows larger and larger over time. Meanwhile, the semiminor axis b steadily decreases, thereby making the orbit more and more elliptical. Consequently, the eccentricity, ε, of the orbit, given by

$$\varepsilon = \sqrt{1 - \left(\frac{b}{a}\right)^2} \quad , \tag{1}$$

steadily increases during this time, starting at zero and increasing toward unity, until a particular critical value, which we will call $\varepsilon_{\mathrm{crit},n}$, is reached. At that moment, the classical electron falls out of subharmonic resonance and the orbit falls into steady decline. As shown in the present article, $\varepsilon_{\mathrm{crit},n}$ is only dependent on the particular subharmonic state, n, mentioned above. Thus, for any subharmonic resonance of state $n = 2$ (incident light's frequency is twice that of the electron's orbital frequency), one obtains the rather surprising result that the transition from resonance to orbital decay occurs when the eccentricity reaches the value of $\varepsilon_{\mathrm{crit},2} \approx 0.554$. This result holds under a wide range of conditions, to be qualified somewhat in Sec. V. For example, this transition point holds for any resonant semimajor axis a value, such as 1 Å or 10 Å, that satisfies the classical orbit criteria. Likewise, for $n = 3$, $\varepsilon_{\mathrm{crit},3} \approx 0.671$; for $n = 4$, $\varepsilon_{\mathrm{crit},4} \approx 0.732$. Simulation results will show this behavior. In addition, we will derive analytically why these specific $\varepsilon_{\mathrm{crit},n}$ values occur, arriving at an analytic expression for them.

Rydberg atomic systems, and the hydrogen atom in particular, are of interest for a number of reasons. Paths to ionization have subtleties not fully investigated before; related work to that presented here shows that such paths can be analyzed more deeply and thereby possibly be controlled better, at least in a statistical sense, which might be used to advantage in plasma devices and the important area of plasma etching. In addition, it appears that the "state" of a Rydberg atom can be controlled, which prompts the ideas of "reading" and "writing" information, or changing the state, of such a system. By this we mean not just the large quantum number for a highly excited Rydberg atom, as at this point such a state is nearly a continuum of states, but as discussed here, the classical subharmonic resonances that can result in semi-stable states for lengths of time.

Interesting and related experimental work related to the theory and simulation work reported here, has been carried out by others. For example, there appears to

be suggestive connections with the experimental work in [7], [8], [9] involving applied microwaves perturbing atomic Rydberg systems. Their work involve both ionization and stabilization effects that depend on many critical factors for Rydberg atoms.

Finally, the hydrogen atom has long been a key physical system for our understanding, due to it's simplicity, yet rich history of physical analysis [10]. Moreover, the work presented here may well be helpful in a deeper understanding of the connections and differences between the theory of stochastic electrodynamics (SED) [11],[12] and both quantum theory and quantum phenomena, and for being applicable to systems other than linear harmonic oscillators [13]. Some work seems to indicate that the ground state of hydrogen may be understood to some extent by SED [14], [6], [15], [16], [17].

A very quick way to clarify this discussion on subharmonic resonance, before getting into the full analysis, is to simply show some simulations of this phenomena. We will turn to that next. After this brief set of illustrations, an outline of the remainder of this article, including equations of motion, analysis, and computational method, will be provided.

Figures 1a-h illustrate most of the essential points that will be brought out here. Figures 1a-f pertain to one arbitrary $n = 2$ subharmonic resonance simulation, while Figs. g,h are of a similar $n = 2$ situation, but with a five times as large as the former, just to illustrate that these size changes hold. In the first case, the classical electron is started in a circular orbit, with radius 1.08 Å. Now, to be really classical, where quantum effects would be minimized, then it is true that this orbit should be chosen much larger. However, the same effect illustrated here will still occur if the Lorentz-Dirac equation [18],[19] is taken to be the governing equation of motion, as has been verified by numerous simulation tests of ours; the only restriction is that one should expect this subharmonic resonance to hold, physically, at the larger radius connections, where the correspondence principle provides the connection between large quantum numbers and continuous classical trajectories. The reason for showing smaller radii is that simulations certainly run much faster at small radii, plus if SED is to be explored further to understand better about it's applicability and deficiencies, then the smaller radii are of most interest.

In Fig. 1a, the y-axis shows the semimajor, a, and semiminor, b, axes of the classical electron's orbit. Since the orbit starts in a circle, then $a \approx b$, up until $t \approx 0.42 \times 10^{-10}$ s. During each orbit, namely, about 10^5 orbits up until the resonance point at $t \approx 0.42 \times 10^{-10}$ s, energy in the form of classical electromagnetic radiation is constantly being given off, resulting in the orbit constantly decreasing from $a = 1.08$ Å to where the $n = 2$ subharmonic resonance occurs. Note that during this entire simulation, a circularly polarized plane wave is acting, however, it has a very weak effect on the trajectory until a decreases to the resonance point, at which time a very sharp resonance can be seen. In this simulation, the amplitude of the electric field of the CP wave was chosen to be $A = 1000$ statvolt/cm, in cgs units (we will use cgs units throughout). The angular frequency of the CP wave, in this simulation, is given by $\omega_1 = \left(\frac{e^2}{ma_1^3}\right)^{1/2}$, where, in cgs units, the charge of the classical electron is $e = 4.80298 \times 10^{-10}$esu, the mass of the electron is $m = 9.1091 \times 10^{-28}$ g, and here a_1, for this simulation, was chosen to be 0.6 Å $= 0.6 \times 10^{-8}$ cm. Thus, $\omega_1 = 3.4241 \times 10^{16}\,\mathrm{s}^{-1}$. The $n = 2$ net angular frequency resonance, when a CP wave is applied with an angular frequency ω_1, is given by $\omega_2 = \frac{\omega_1}{2}$, which occurs if $\omega_2 = \left(\frac{e^2}{ma_2^3}\right)^{1/2} = \frac{1}{2}\omega_1 = \frac{1}{2}\left(\frac{e^2}{ma_1^3}\right)^{1/2}$, or $a_2 = a_1 \times 2^{2/3}$. For this simulation, that means $a_2 = 0.6$ Å $\times\, 2^{2/3} \approx 0.9524$ Å. As

can be seen from Fig.1a, this is precisely where this resonance takes place, and indeed holds to many decimal places if we were to zoom in on the plot much closer.

At this point, the applied CP wave has a clear effect on the orbit. The semimajor axis a no longer decays, but stays fairly constant, while the semiminor axis, b, begins a steady decline. The orbit abruptly changes from a circular one ($\varepsilon = 0$) during the initial decay period between $0 \leq t \lessapprox 0.42 \times 10^{-10}$ s, to becoming more and more elliptical between 0.42×10^{-10} s $\lessapprox t \lessapprox 1.07 \times 10^{-9}$ s. Figure 1b shows this behavior. During this resonance period, about 2.8×10^6 orbits occur, each with a period of approximately 3.67×10^{-16} s.

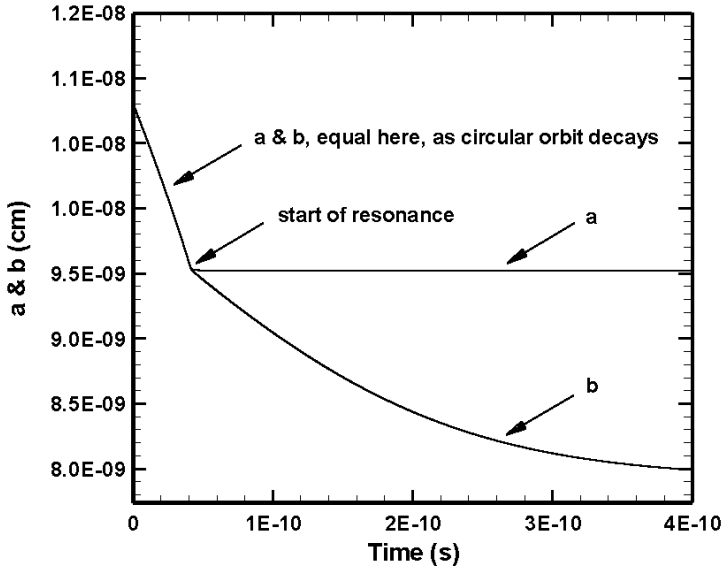

Fig. 1 All of the Figs. 1a to 1f were carried out under the same conditions, namely, $a_1 = 0.6\,\text{Å}$, ω_1 for the CP wave was $\omega_1 = \left(\frac{e^2}{ma_1^3}\right)^{1/2}$, the orbit began at $a = 1.08\,\text{Å}$ in a circular orbit, so $\varepsilon_{\text{initial}} = 0$, $A = 1000$ statvolt/cm, and $a_2 = a_1 2^{2/3} \approx 0.9524\,\text{Å}$, and $\alpha = 0$ in (12) and (13). **Fig. 1a** Plots of $a\,(t)$ and $b\,(t)$ vs. t, for the start of an $n = 2$ subharmonic resonance, shown to the end of the resonance in Fig. 1b. The key points to note are that the orbit initially decays, during which $a = b$, then a sharp change occurs when resonance is reached at $a_2 = a_1 2^{2/3} = 0.9524\,\text{Å}$, after which a stays flat, while b decreases.

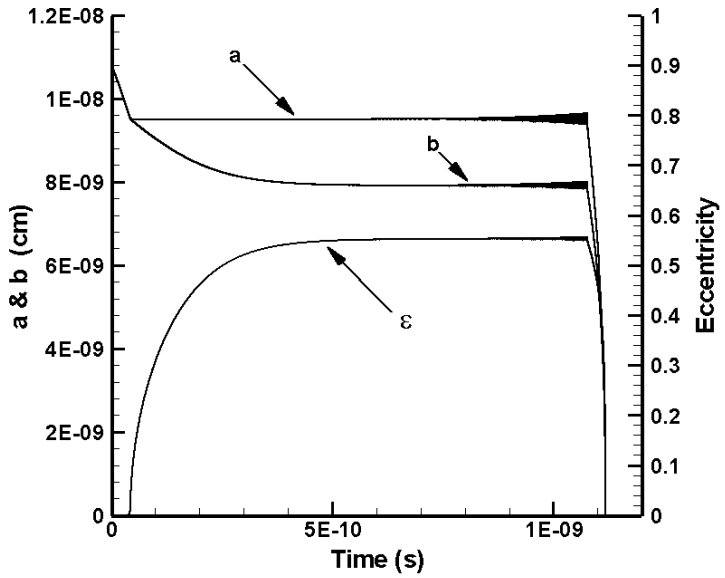

Fig. 1b Plots of a, b, and ε vs. t, from start to finish, where the orbit begins in a decaying circular orbit (Fig. 1a), then proceeds to the start of the $n = 2$ subharmonic resonance, then to the end of this resonance, finally ending in orbital decay. As will be shown, both analytically and via simulation, $\varepsilon_{\mathrm{crit},n} \approx 0.5542$ for $n = 2$, is the eccentricity when the transition of orbital resonance to decay occurs.

Each of the curves, a vs. t, b vs. t, and ε vs. t, contain a fluctuation to them that increasingly grows larger with time. This can be seen by the increasing "blocky" width of each of these lines gradually increasing from the point of resonance $t \approx 0.42 \times 10^{-10}$ s, to when decay eventually sets in at about $t \approx 1.07 \times 10^{-10}$ s. This growing width of each of these three curves contains a very fine oscillating line, growing in amplitude as time increases. To illustrate, Fig. 1c focuses closely in on a vs. t at $t \approx 8 \times 10^{-10}$ s, where a periodic oscillation of a vs. t is seen, constituting the source of the blocky curve in Fig. 1b that grows in width until the decay point is finally reached. The oscillatory nature of a vs. t for this $n = 2$ subharmonic resonance has many similar features to the $n = 1$ resonance analyzed in detail in Refs. [2],[4],[5], in that as A grows, the period of the oscillation in Fig. 1c decreases and the amplitude of the oscillations increases.

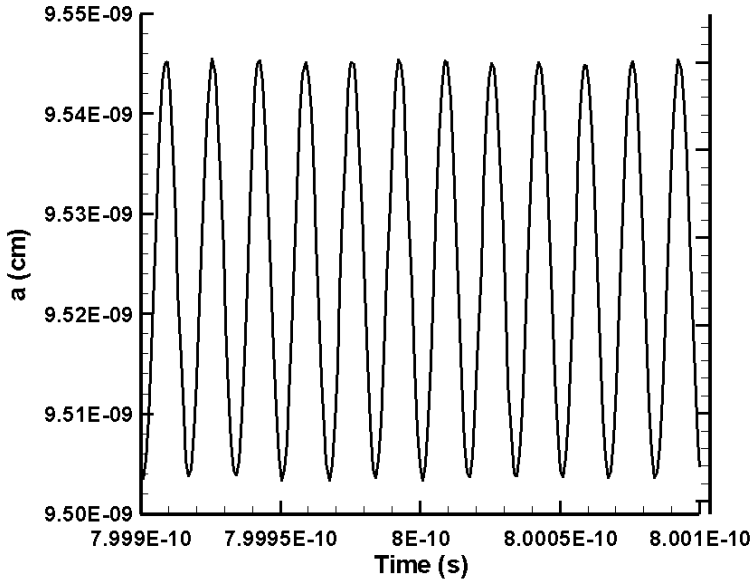

Fig. 1c This plot focuses in on the a vs. t curve in Fig. 1b at about 75% into the subharmonic resonance, at $t \approx 8 \times 10^{-10}$ s. At this scale of the plot, the variation in a looks large, but it is only about a $\pm 0.2\%$ variation in $a\,(t)$. By the point in Fig. 1b where orbital decay sets in, this variation in $a\,(t)$ rises to about a $\pm 1.4\%$ variation. However, the larger A is, the larger will be this variation. Aside: for each full oscillation of $a\,(t)$ in this figure, there are approximately 46 orbital periods at this point in time.

Other than the magnitude of A effecting the fluctuation amplitude of $a\,(t)$, most other features of this resonance remain independent of A (provided it is above a critical value), namely: the resonance at $a_2 = 0.9524\,\text{Å}$ still occurs at this precise value of $a_1 n^{2/3}$, where $n = 2$; the center of the a vs. t slightly fluctuating curve remains quite flat; and resonance stands out as a clear feature, although decay always eventually sets in. The time in resonance before decay sets in certainly depends on A as well as the initial phase α between the CP wave and the orbit, all very similar to the studies carried out on primary ($n = 1$) resonance in previous studies [4],[5], where the orbital and CP wave period are essentially the same. In addition, the length of time in resonance also depends on the starting point of a above the resonance point, and if the initial orbit is circular or has some degree of ellipticity.

Figure 1d examines the basic behavior of the eccentricity. When resonance sets in, ε increases in value as the orbit becomes more elliptical. Also, the ε vs. t curve widens in width as the decay point is approached, due to the increasing oscillation amplitude of ε. After the decay transition point and the orbit changes from one of resonance to that of decay, ε decreases rapidly toward zero, meaning a circular orbit, as discussed in [3].

Figure 1e clarifies some of the points on fluctuations of $\varepsilon\,(t)$, as it examines the point in Fig. 1d where orbital decay begins. The oscillations of ε are largest right before the decay point. A critical change occurs when the larger oscillations to the left "close over at the top," becoming smaller humped oscillations on the right, that now decrease in both amplitude, and average value. From this point on, the CP plane wave loses it ability to remain in phase with the orbit. The amount of positive energy pumped into the orbit decreases, on average, while the amount of negative work increases, as seen in the degree that the CP electric field pushes and opposes the electron along its trajectory. Thus, for $1.07385\times10^{-10}\,\mathrm{s} \lessapprox t$, little to no net energy is gained from the CP electric field, as the orbiting electric and CP field become unable, on average, to remain in a net positive energy phase condition. Consequently, the radiation reaction of the electron, corresponding to the electron emitting electromagnetic radiation, results in the orbit returning to one of steady decay. If we were to show the oscillations in the decaying curve farther out to the right in Fig. 1e, they become smaller and smaller, the farther away from the resonance point.

However, perhaps the most significant point of Fig. 1e is the value $\varepsilon_{\mathrm{crit},n} \approx 0.5542$, for this $n = 2$ simulation. It turns out that whether we repeat this simulation for $a_2 = 2\,\text{Å}$, $10\,\text{Å}$, $20\,\text{Å}$, etc., $\varepsilon_{\mathrm{crit},2}$ is independent of the subharmonic resonance point, for the case of an initial circular orbit that decays into the resonance point. . This will be deduced analytically in Sec. IV, and has the remarkable property that it appears to hold for all other $n = 2$ situations, aside from a few points to be discussed in Sec. V. Moreover, Sec. V will address the $n = 4, 5, 6$, subharmonic resonance situations as well.

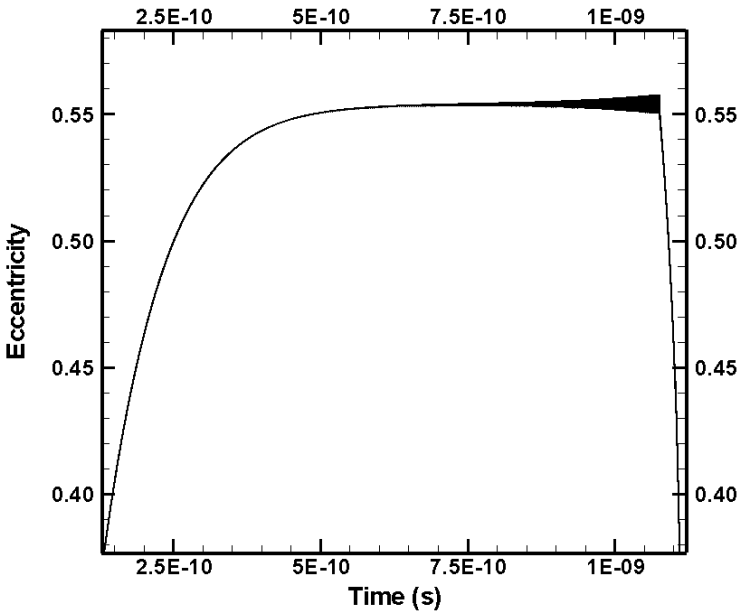

Fig. 1d Plot of $\varepsilon\,(t)$ vs. t, containing the same information as in the $\varepsilon\,(t)$ curve in Fig. 1b, but now focusing in at the point leading up to decay and showing more

clearly the widening of the curve, until decay sets in. Once $\varepsilon \approx 0.5542$ is reached, ε then rapidly decays toward zero, a circular orbit.

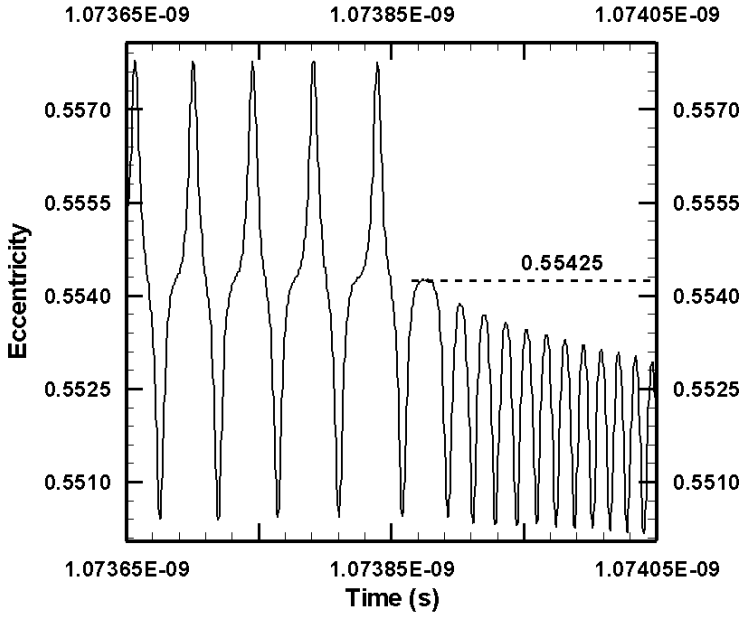

Fig. 1e This plot of $\varepsilon(t)$ vs. t, focuses in at the point where the widening curve in Fig. 1d, changes to a decaying orbit. For $t \lesssim 1.07385 \times 10^{-9}$ s, the oscillations have lower and upper humps that look something like a "pinched" sine wave. However, at $t \approx 1.07385 \times 10^{-9}$ s, the top peaks pinch off entirely, leaving the smaller, decaying oscillations that can be seen for $1.07385 \times 10^{-9}\,\text{s} \lesssim t$. Similar "signatures" of this behavior also appear for $a(t)$, $b(t)$, and energy and angular momentum. Far to the left of the decay point, the oscillations of these variables look more like Fig. 1c, but the closer to the decay point, the more "pinched" become the peaks and valleys, until decay sets in. The $\varepsilon_{\text{crit},2}$ point noted here, of ≈ 0.5542, will agree closely with later analytical results.

Figure 1f shows two plots, the top one being the potential plus kinetic energy of, $E(t) = -\frac{e^2}{r(t)} + \frac{1}{2}m\left|\mathbf{v}(t)\right|^2$, as a function of time, t, where r is the radial distance to the nucleus and $\mathbf{v}$ is the classical electron's velocity. The bottom curve is $\mathbf{F} \cdot \mathbf{v}$ vs. t, where $\mathbf{F}$ is the sum of the CP wave and radiation reaction forces. The narrow time region shown in Fig. 1f of 2.65×10^{-13} s (same interval as in Fig. 1e) encompasses the moment when the orbit in Fig. 1b changes from one of resonance to that of decay.

The top curve in Fig. 1f of $-\frac{e^2}{r(t)} + \frac{1}{2}m\left|\mathbf{v}(t)\right|^2$, closely matches the approximate energy $-\frac{e^2}{2a(t)}$, where $a(t)$ is of course the relatively slowly changing semimajor axis of the approximate elliptical orbit, as the elliptical orbit slowly grows and shrinks.

Indeed, at the scale in Fig. 1f, $E(t) = -\frac{e^2}{r(t)} + \frac{1}{2}m\left|\mathbf{v}(t)\right|^2$ and $-\frac{e^2}{2a(t)}$, are virtually indistinguishable from each other. This fact will be illustrated in Sec. IV and will be used to advantage there when deducing values for $\varepsilon_{\mathrm{crit},n}$.

For the situation of Fig. 1f, $a \approx a_2 = 0.6 \times 2^{2/3}\,\text{Å} = 0.9524\,\text{Å}$, with a small oscillation of about $\pm 1.4\%$ (this was measured by zooming in on Fig. 1b) about this value at the onset of orbital decay, so the center of E vs. t is very close to $-\frac{e^2}{2a_2} = -1.211 \times 10^{-11}\,\text{erg}$, as can be seen in Fig. 1f. The bottom curve is the work per unit time put into the trajectory. When in resonance, the sign of this curve changes roughly n times per orbit when in an n^{th} subharmonic resonance, since the orbital period is close to n times the period of the CP wave. With about 720 orbital periods in the $2.65 \times 10^{-13}\,\text{s}$ time interval in Fig. 1f, and roughly twice as many sign changes in $\mathbf{F} \cdot \mathbf{v}$ for this $n = 2$ subharmonic resonance, the plot of $\mathbf{F} \cdot \mathbf{v}$ vs. t in the bottom of Fig. 1f is quite complicated, considerably more so than $n = 1$ resonance situations discussed in earlier references [2],[4],[5], where the times between sign changes of $\mathbf{F} \cdot \mathbf{v}$ may last tens to hundreds of orbits before changing.

A white line was drawn across the bottom plot in Fig. 1f for when $\mathbf{F} \cdot \mathbf{v} = 0$. If one compares the bottom, rapidly changing plot, to the top plot, one can see that when the average of $\mathbf{F} \cdot \mathbf{v}$ over a short time interval is positive, then $E(t)$ in the top plot increases, and when the average of $\mathbf{F} \cdot \mathbf{v}$ over a short time interval is negative, then $E(t)$ decreases. This is similar to the $n = 1$ resonance situation, but also significantly different in that here, the average over many plus and minus fluctuations of the power $\mathbf{F} \cdot \mathbf{v}$ is the key entity that leads to changes in $E(t)$. We will make use of this aspect when carrying out the analytic predictions of $\varepsilon_{\mathrm{crit},n}$ in Sec. IV.

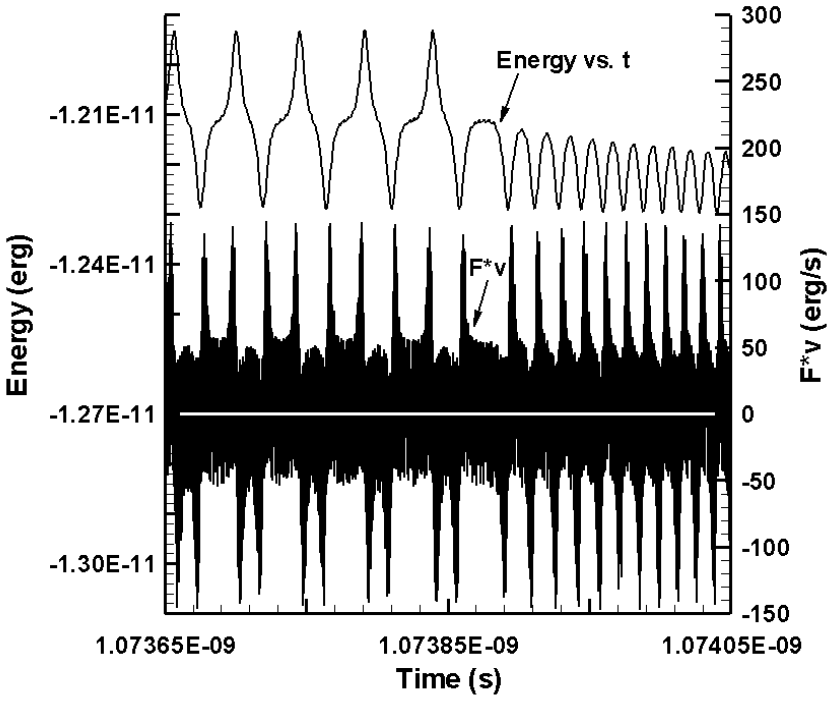

Fig. 1f The top plot is of $E(t) = -\frac{e^2}{r(t)} + \frac{1}{2}m\left|\mathbf{v}(t)\right|^2$, which will be shown later in Sec. IV, to be close to $-\frac{e^2}{2a(t)}$ for the range of values of A considered here in this article. Of course these would be exactly equivalent if the CP wave and radiation reaction were not present. The bottom plot is of $\mathbf{F}\cdot\mathbf{v}$ vs. t, where $\mathbf{F}$ is the sum of the CP wave and radiation reaction forces. This "power" of the work per time by the CP wave and radiation reaction is of course what changes $E(t)$ in the top curve; if these two forces were zero, then $E(t)$ would be a constant and we would be back to a pure Coulombic elliptical orbit that does not change. The fast fluctuations of $\mathbf{F}\cdot\mathbf{v}$ create a complicated scenario, but by averaging in time over short regions, one can see that when $\mathbf{F}\cdot\mathbf{v}$ is more positive than negative, then $E(t)$ increases, and vice versa. The white line indicates when $\mathbf{F}\cdot\mathbf{v} = 0$, to help make it easier to see this last connection. The time span here is the same as in Fig. 1e, so right when the orbit changes from a state of resonance to one of decay.

Lastly, Figs. 1g and 1h correspond to an $n = 2$ subharmonic resonance with an a_2 value that is five times as large as the situation in Figs. 1a-f. Figure 1g shows a vs. t and ε vs. t for the a_2 resonance situation of $a_2 = 3.0\times 2^{2/3}\,\text{Å} = 4.7622\,\text{Å}$, which should be compared with the plots in Fig. 1b for $a_2 = 0.6\times 2^{2/3}\,\text{Å} = 0.9524\,\text{Å}$. Likewise, Fig. 1h focuses in on the ε vs. t point where orbital decay sets in; this figure corresponds to Fig. 1e. The $n = 2$ situation of $a_2 = 3.0\times 2^{2/3}$ Å in Figs. g,h and of $a_2 = 0.6\times 2^{2/3}$ Å in Figs. 1b,e, contain essentially the same $\varepsilon_{\text{crit},2}$ value at the point when orbital resonance

changes to orbital decay, despite the large difference in semimajor axis. This is one of the key points to be shown in the analytical derivation in Sec. IV.

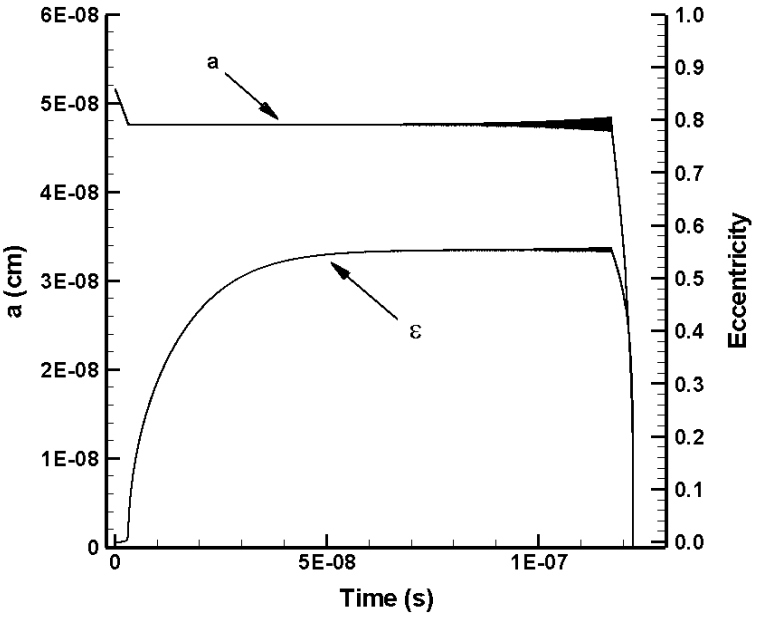

Fig 1g This $n = 2$ subharmonic resonance condition has an a_2 value that is five times as large as in Figs. 1a-f. Here, $a_1 = 3.0\,\text{Å}$ and $a_2 = a_1 2^{2/3} = 4.7622\,\text{Å}$, while $A = 50$ statvolt/cm, $\varepsilon_{\text{initial}} = 0$, $\alpha = 0$. The ε vs. t curve is also shown. Note that $\varepsilon = 0$ (a circular orbit) while a decreases until $a\,(t)$ hits the $n = 2$ resonance, at which point $\varepsilon\,(t)$ starts increasing.

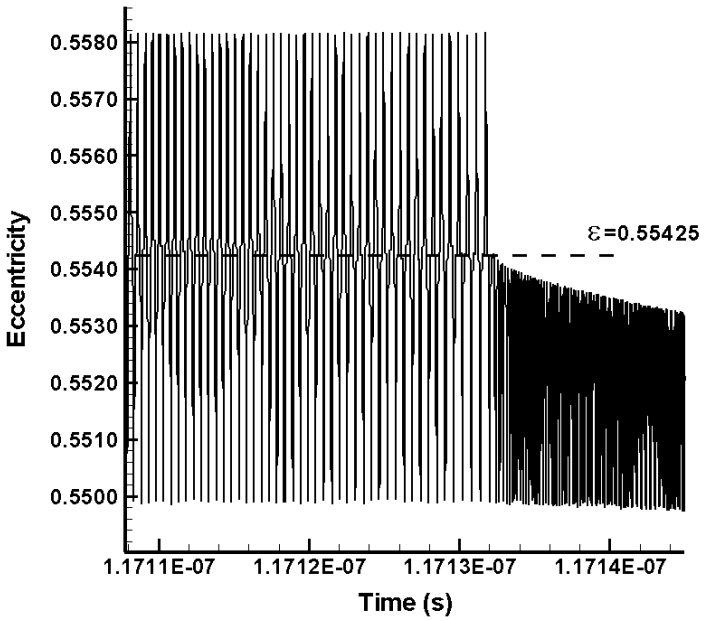

Fig 1h This plot of $\varepsilon\,(t)$ vs. t, focuses in at the point in Fig. 1g where the orbit changes from one of resonance to orbital decay. Compare with Fig. 1e, where $a\,(t)$ was about 1/5 times the size. In both cases, $\varepsilon_{\mathrm{crit},2}$, the eccentricity at the point between resonance and decay, is nearly identical. Later analytical results in Sec. IV will establish this connection in a deeper manner.

Finally, soon we will examine conditions such as an $n = 3$ or $n = 4$ subharmonic resonance, where $\omega_3 = \frac{1}{3}\omega_1$, $\omega_4 = \frac{1}{4}\omega_1$, etc., where $\omega_1 = \frac{f_1}{2\pi}$ is the net angular frequency of the CP wave, f_1 is the CP wave's frequency, $\omega_3 = \frac{f_3}{2\pi}$, $\omega_4 = \frac{f_4}{2\pi}$, and f_3 and f_4 are the net orbital frequencies of the classical electron orbit. We will see that similar scenarios to our $n = 2$ example will play out. We will find a unique value of $\varepsilon_{\mathrm{crit},3} \approx 0.669$ for all $n = 3$ subharmonic resonances, no matter the orbital resonance size. For $n = 4$, the basic behavior will again hold, but now $\varepsilon_{\mathrm{crit},4} \approx 0.732$. These points will be brought out, with some caveats, and analyzed in more detail in subsequent sections.

The plots shown above are in sharp contrast to the work shown in Ref. [1], where the analysis concentrated on radius and energy versus time, as opposed to recognizing that the orbits were changing from circular to becoming more elliptical in nature. Consequently, the previous work did not touch on the essentially constant semimajor axis during resonance, nor the critical values of ε when decay eventually arose.

The remainder of the article proceeds as follows. Section II turns to the specific equations governing this phenomena and our method for extracting the near elliptical parameters for the orbits. More simulation results are shown in Section III, such as the effect of increasing A for various subharmonic resonance cases, and showing the unique result of $\varepsilon_{\mathrm{crit},n}$. Section IV then analyzes and derives a formula for $\varepsilon_{\mathrm{crit},n}$ for different subharmonic resonances Section V comments on some physical aspects and

caveats that need to be mentioned about this work. Concluding comments are in Sec. VI.

2 Equations of motion and elliptical parameter extraction

The motion of the classical electron, with point charge $-e$ and mass m, no spin, and for nonrelativistic speeds, while bound to an infinitely massive center with opposite point charge $+e$ (nucleus), is described by the nonrelativistic Lorentz-Dirac (LD) equation of motion in cgs units: [18],[20]:

$$m\frac{d^2\mathbf{z}}{dt^2} = -e^2\frac{\mathbf{z}}{|\mathbf{z}|^3} + \frac{2e^2}{3c^3}\frac{d^3\mathbf{z}}{dt^3} - e\mathbf{E}_{\rm CP}\left[\mathbf{z}\left(t\right),t\right] - \frac{e}{c}\frac{d\mathbf{z}}{dt}\times\mathbf{B}_{\rm CP}\left[\mathbf{z}\left(t\right),t\right] \quad . \tag{2}$$

Here, m is the mass of the classical electron, $-e$ is its charge, c is the speed of light, $-e^2\frac{\mathbf{z}}{|\mathbf{z}|^3}$ is the Coulombic binding force, $-\frac{2e^2}{3c^3}\frac{d^3\mathbf{z}}{dt^3}$ is the nonrelativistic radiation reaction term, and $\mathbf{E}\left[\mathbf{z}\left(t\right),t\right]$ and $\mathbf{B}\left[\mathbf{z}\left(t\right),t\right]$ are additional electric and magnetic fields acting on the system, acting via the Lorentz force on the motion of the particle. Certainly other radiation fields than a CP wave can be examined, but this study concentrates only on the effects of a CP wave. Section VI comments further on this emphasis, with qualitative discussions on other choices.

In place of (2), the full relativistic LD equation [18] can certainly be used, but for typical Rydberg orbits, where the orbit radius is quite large, it is quite unnecessary as the classical electron's speed $|\mathbf{v}|$ is so small compared to the speed of light. For circular orbits, only when the radius r shrinks to about $0.28\,\text{Å}$ is $v/c \approx 0.01$, or 1%, and not until r is nearly 100 times smaller than that does v/c reach about 0.1, or 10%, where relativistic corrections are then clearly needed. For elliptical orbits, the need for relativistic corrects can occur earlier, as the maximum speed in an elliptical orbit from the nonrelativistic and the classical Kepler-like equation of

$$m\frac{d^2\mathbf{z}}{dt^2} = -e^2\frac{\mathbf{z}}{|\mathbf{z}|^3} \quad , \tag{3}$$

is given by

$$v_{\max} = \frac{e}{m^{1/2}a^{1/2}}\left(\frac{1+\varepsilon}{1-\varepsilon}\right)^{1/2} \quad . \tag{4}$$

When $\varepsilon = 0$, the orbit is circular, $v_{\max}/c = \frac{e}{(ma)^{1/2}c}$, and it is this quantity that equals 0.01 when $a \approx 0.28\,\text{Å}$, as mentioned before. However, as can be seen from (4), for extremely elliptical orbits, where ε approaches 1, then the full relativistic LD equations should be used. We will not be examining such situations here, nor examining very small a situations.

The "damping" term in (2) of $\frac{2e^2}{3c^3}\frac{d^3\mathbf{z}}{dt^3}$ is much weaker than other forces, due to the extremely small magnitude of

$$\tau \equiv \frac{2e^2}{3c^3} = 6.266031\times10^{-24}\,\text{s} \quad . \tag{5}$$

Moreover, the magnitude of the Lorentz force of the CP plane wave acting on the electron, is typically orders of magnitude smaller than the Coulombic force of the nucleus, $-e^2\frac{\mathbf{z}}{|\mathbf{z}|^3}$, acting on the electron, at least for the simulation examples considered

here, as well as what might normally be encountered experimentally. Hence, as is often done in such problems, the small term $\frac{2e^2}{3c^3}\frac{d^3\mathbf{z}}{dt^3}$ is approximated by [18],[20]:

$$\frac{2e^2}{3c^3}\frac{d^3\mathbf{z}}{dt^3} = \frac{2e^2}{3c^3}\frac{d}{dt}\left(\frac{d^2\mathbf{z}}{dt^2}\right) \approx \frac{2e^2}{3c^3}\frac{d}{dt}\left(-e^2\frac{\mathbf{z}}{|\mathbf{z}|^3}\right)$$
$$= -\frac{2e^4}{3c^3}\left[\frac{\frac{d\mathbf{z}}{dt}}{|\mathbf{z}|^3} - \frac{3\mathbf{z}(\mathbf{z}\cdot\frac{d\mathbf{z}}{dt})}{|\mathbf{z}|^5}\right] \quad . \tag{6}$$

The situation considered here is where the orbit of the classical electron begins in the $x-y$ plane and where the CP plane wave is directed in the $-\hat{\mathbf{z}}$ direction toward the $z=0$, $x-y$ plane. The following expressions for the CP electric and magnetic fields are due to two traveling plane waves, one $\frac{\pi}{2}$ with respect to the phase of the other, but both traveling in the $-\hat{\mathbf{z}}$ direction, so $\mathbf{k} = -\hat{\mathbf{z}}\frac{\omega_1}{c}$, where ω_1 is the angular frequency of the incident plane waves. Thus,

$$\hat{\mathbf{k}} = -\hat{\mathbf{z}} = \frac{\mathbf{E}_{\rm CP}\times\mathbf{B}_{\rm CP}}{|\mathbf{E}_{\rm CP}\times\mathbf{B}_{\rm CP}|} \quad , \tag{7}$$

and

$$\mathbf{E}_{\rm CP} = A\left[\hat{\mathbf{x}}\cos\left(\mathbf{k}\cdot\mathbf{z}-\omega_1 t+\frac{\pi}{2}-\alpha\right) - \hat{\mathbf{y}}\cos\left(\mathbf{k}\cdot\mathbf{z}-\omega_1 t-\alpha\right)\right] \quad , \tag{8}$$

$$\mathbf{B}_{\rm CP} = A\left[-\hat{\mathbf{x}}\cos\left(\mathbf{k}\cdot\mathbf{z}-\omega_1 t-\alpha\right) - \hat{\mathbf{y}}\cos\left(\mathbf{k}\cdot\mathbf{z}-\omega_1 t+\frac{\pi}{2}-\alpha\right)\right] \quad . \tag{9}$$

The electric and magnetic fields lie solely in the $x-y$ plane of the orbiting electron, with $\hat{\mathbf{k}}\times\mathbf{E}_{\rm CP} = -\hat{\mathbf{z}}\times\mathbf{E}_{\rm CP} = \mathbf{B}_{\rm CP}$. The electric field vector points and rotates in the counterclockwise direction, with a constant magnitude of A, with the same for the magnetic field, which is perpendicular to the electric field. The phase factor α allows for the situation where the force $-e\mathbf{E}_{\rm CP}$ and the velocity of the electron, $\frac{d\mathbf{z}}{dt}$, are at an angle α at $t=0$. The significant effect of α on length of time to decay was explored in some detail in Ref. [5] for the primary resonance case of $n=1$; the effect can be quite significant. Section VI comments briefly on the interest here for a single CP wave; however, clearly the infinite other types of radiation states possible, simply magnify the phenomena that might occur.

The only force that acts to move the classical electron out of the $x-y$ plane orbit is due to the Lorentz force from the magnetic field, or

$$-\frac{e}{c}\frac{d\mathbf{z}}{dt}\times\mathbf{B}_{\rm CP}\left[\mathbf{z}\left(t\right),t\right] \quad .$$

The magnitude of this force is typically fairly weak force due to the $1/c$ factor. For the length of time of the simulations considered here, the contribution of this force in the z direction, is fairly negligible. It acts to slowly change the planar orbit to a more 3D behavior, but the time scale is quite long.

Consequently, our following analysis will entail the CP fields in the $x-y$ plane at $z=0$. Rewriting slightly:

$$\mathbf{E}_{\rm CP} = A\left[\hat{\mathbf{x}}\cos\left(\omega_1 t-\frac{\pi}{2}+\alpha\right) - \hat{\mathbf{y}}\cos\left(\omega_1 t+\alpha\right)\right] \quad , \tag{10}$$

$$\mathbf{B}_{\rm CP} = A\left[-\hat{\mathbf{x}}\cos\left(\omega_1 t+\alpha\right) - \hat{\mathbf{y}}\cos\left(\omega_1 t-\frac{\pi}{2}+\alpha\right)\right] \quad . \tag{11}$$

Combining (2) with (6), (10) and (11), and writing the equations of motion in the $x-y$ plane using polar coordinates, r and θ, results in:

$$m\left(\ddot{r}-r\dot{\theta}^2\right)=-\frac{e^2}{r^2}+2\tau e^2\frac{\dot{r}}{r^3}+eA\sin\left(\theta-\omega_1 t-\alpha\right) \quad , \tag{12}$$

and

$$m\left(r\ddot{\theta}+2\dot{r}\dot{\theta}\right)=-\tau e^2\frac{\dot{\theta}}{r^2}+eA\cos\left(\theta-\omega_1 t-\alpha\right) \quad . \tag{13}$$

The left side of (12) equals the mass times the acceleration in the positive radial direction; the right side equals the sum of forces in the same direction. The left side of (13) equals the mass times the acceleration in the increasing θ direction; the right side equals the sum of forces in the same direction.

The nonlinear, coupled, ordinary differential equations (12) and (13), second order in time, will be solved numerically here using an adaptive stepsize Bulirsch-Stoer routine [21], similar to the work in [1]. However, here a least squares method was developed and implemented to extract elliptical parameters matching the electron's slowing changing orbit. The premise here is that with the Coulombic potential being the dominant forcing mechanism on the orbit, then the orbit should be essentially elliptical, since from far back with Newton's work, (3) leads to elliptical orbits for bound systems. The CP plane wave is the next strongest force, which can result in the elliptical orbit slowly changing, while the damping term acts to slowly shrink the orbit. Indeed, if no CP wave is present, the damping term slowly collapses any elliptical orbit, making it more circular, and shrinking the radius to zero (for example, see Fig. 4 in [3], where this effect is clearly shown). Of course, when the radius becomes too small, perhaps less than about 0.1 Å ($v_{\max}/c\approx 0.017$), then the relativistic Lorentz-Dirac equation should be used.

Thus, $r\left(t\right)$ and $\theta\left(t\right)$ were numerically solved for here, plus a parameter extraction method was implemented to approximate the trajectory as an ellipse that slowly rotates and changes in the size of its two axes. The parameters extracted were the approximate values for the semimajor axis, a, the eccentricity, ε, and the angle, θ_0, of the center axis of the ellipse with respect to the x axis. From a and ε, one can obtain the semiminor axis, b, from (1). The radius of the orbit, from the nucleus center of the Coulombic force (again, approximating that this much more massive center does not move), can be written as a function of θ via

$$r\left(\theta\right)=\frac{a\left(1-\varepsilon^2\right)}{1-\varepsilon\cos\left(\theta-\theta_0\right)} \quad , \tag{14}$$

where $x=r\cos\left(\theta\right)$ and $y=r\cos\left(\theta\right)$. The above expression, when a, ε, θ_0 are constants, is the geometrical solution to the Kepler-Coulombic (3) equation. The parameters a, ε, and θ_0 were obtained via the least squares method described in [3], that keeps track of r and θ values of the orbiting particle, for N points, where N is made large enough to encompass at least one or more orbits. Thus, a, ε, and θ_0 were treated as slowly changing parameters in time to match the approximate elliptical orbit at any instant. These parameters were extracted by rewriting (14) as

$$\frac{1}{r}=\frac{1}{a\left(1-\varepsilon^2\right)}-\left[\frac{\varepsilon\cos\left(\theta_0\right)}{a\left(1-\varepsilon^2\right)}\right]\cos\left(\theta\right)-\left[\frac{\varepsilon\sin\left(\theta_0\right)}{a\left(1-\varepsilon^2\right)}\right]\sin\left(\theta\right) \quad , \tag{15}$$

and then making a table of $1/r$, $\cos(\theta)$, and $\sin(\theta)$ for N points, sequentially in time. The parameters

$$P_1 \equiv \frac{1}{a\,(1-\varepsilon^2)} \quad , \tag{16}$$

$$P_2 \equiv -\frac{\varepsilon\cos(\theta_0)}{a\,(1-\varepsilon^2)} \quad , \tag{17}$$

$$P_3 \equiv -\frac{\varepsilon\sin(\theta_0)}{a\,(1-\varepsilon^2)} \quad , \tag{18}$$

were then obtained by least-squares methods. From P_1, P_2, and P_3, then a, ε, and θ_0 were obtained.

3 Simulation Results

Similar to the $n = 2$ example in Fig. 1 in Sec. I, Fig. 2 below shows a similar scenario for a subharmonic resonance of $n = 3$, where the incident CP wave has a frequency three times that of the electron's orbital frequency. In Fig. 2a, the electron's orbit started in a circular orbit with $r = 0.7\,\text{Å}$. To "catch" an electron in an $n = 3$ state, versus an $n = 2$ one, for similar radii values, requires much stronger CP plane wave amplitudes, as discussed in [1] (*e.g.*, see Fig. 4 in [1]). Here, $A = 35,000$ statvolt/cm was used. If A is too low, then the resonance condition is not met, and the electron will continue to decay through the $n = 3$ resonance point. A related important characteristic feature is that the larger A is above the critical value to "catch and hold" the decaying orbit, the wider the a vs. t resonance envelope becomes as t increases, as will be clearly seen shortly in Fig. 3a.

In Fig. 2, the angular frequency of the CP wave was chosen to be $\omega_1 = \left(\frac{e^2}{ma_1^3}\right)^{1/2}$, with $a_1 = 0.3\,\text{Å}$, so $\omega_1 = 9.6848\times10^{16}\,\text{s}^{-1}$, while the resonant orbital angular frequency was $\omega_3 = \frac{1}{3}\omega_1$. As seen in Fig. 2a, the electron decays from the starting point of $r = 0.7\,\text{Å}$, despite the CP wave constantly acting. During this initial decay period, the electron's motion is barely effected by the CP wave. Although not shown, if plots with $A = 0$ and $A = 35,000$ statvolt/cm, or other values of A, were superimposed, little difference would be seen until resonance is reached. However, when the semimajor axis (which up to now is the same as the radius) decays to the point of $a_3 = a_1 \times 3^{2/3} = 0.6241\,\text{Å}$, then the CP wave's action on the orbit becomes very significant. The decaying orbit stops, the semimajor axis a vs. t becomes fairly flat, although with an envelope, due to oscillations in a vs. t, that widens as t increases. As in Fig. 1 for the $n = 2$ case, b decreases over time, resulting in the eccentricity $\varepsilon = \sqrt{1-\left(\frac{b}{a}\right)^2}$ increasing. Prior to reaching the $n = 3$ resonance point, $\varepsilon \approx 0$, as the orbit is essentially circular. After reaching the resonance point, ε increases steadily until the orbit goes back into a decaying mode, which is reached for $n = 3$ conditions when $\varepsilon \approx 0.6706$, to be deduced analytically in Sec. IV.

Figure 2a also contains a fairly typical plot of θ_0, before, during, and after resonance. Until resonance is reached, $\theta_0 \approx 0$. After the start of resonance, which occurred at about $t \approx 1.1\times10^{-11}\,\text{s}$, the orbit becomes more and more elliptical and the axis of the orbit undergoes rotations adding up to about 2800 radians, or about 446 revolutions. Of course during this resonance period the classical electron undergoes orders

of magnitude more revolutions about the nucleus, namely, about 6×10^5 revolutions, or about a factor of 1000 for this particular example.

Resonance makes the axis of the orbit rotate, with larger amounts of rotation occurring as A becomes larger. Before and after resonance, however, the axis rotations essentially stop, which makes sense since at these points, the orbit is little influenced by the CP wave and is largely dictated by the $1/r^2$ Coulombic attraction to the nucleus, which of course results in the well known elliptical orbit behavior explained so long ago by Newton.

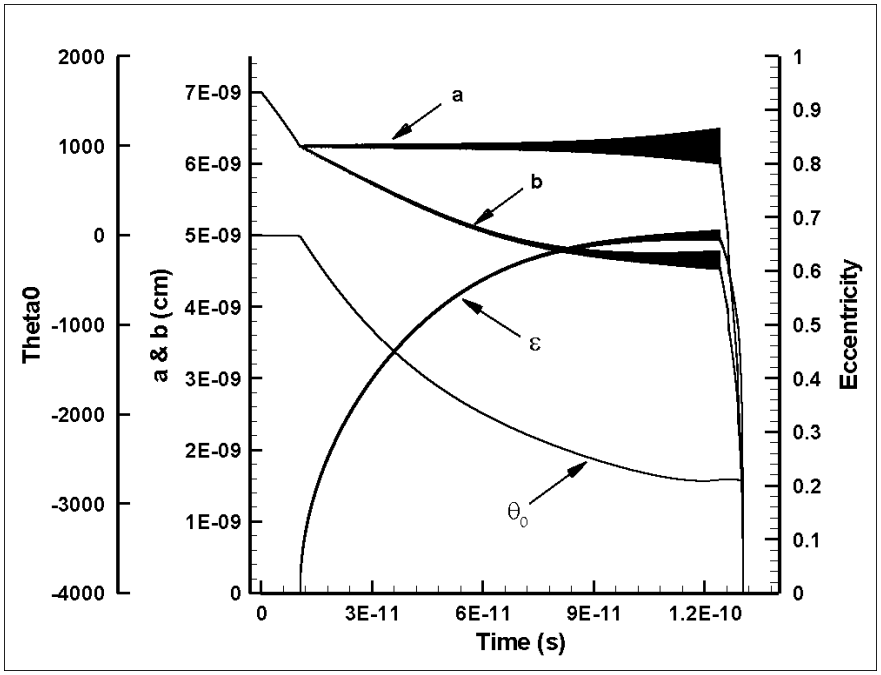

Fig. 2a Here, $A = 35,000$ statvolt/cm, $a_1 = 0.3\,\text{Å}$, $a_3 = 0.3 \times 3^{2/3}\,\text{Å} = 0.6240\,\text{Å}$, $a_{\text{initial}} = 0.7\,\text{Å}$, $\varepsilon_{\text{initial}} = 0$, and $\alpha = 0$ in (12) and (13). The classical electron orbit begins in a spherical orbit at $a = 0.7\,\text{Å}$, but upon hitting resonance at $a_3 = 0.6240\,\text{Å}$,the orbit sharply transitions into one of resonance, where a remains "constant with growing fluctuations," for about 1.2×10^{10} s, until orbital decay starts. $a\,(t)$, $b\,(t)$, $\varepsilon\,(t)$, and $\theta_0\,(t)$ are shown in this plot.

Figure 2b shows a "focused-in" view of the a vs. t curves during the period from when the $n = 3$ resonance changes into a decaying orbital trajectory. As can be seen, two other resonances, not really visible in Fig. 2a, are past through, namely, the $a_2 = a_1 2^{2/3} = 0.4762\,\text{Å}$ and $a_1 = 0.3\,\text{Å}$ resonance points. The conditions imposed by A, ε, α at these resonance points was insufficient to significantly delay further decay, unlike the $a_3 = 0.6240\,\text{Å}$ point. Ultimately, the orbit must have a close correlation in phase with the CP wave for sustained resonance to occur. More will be said about this later.

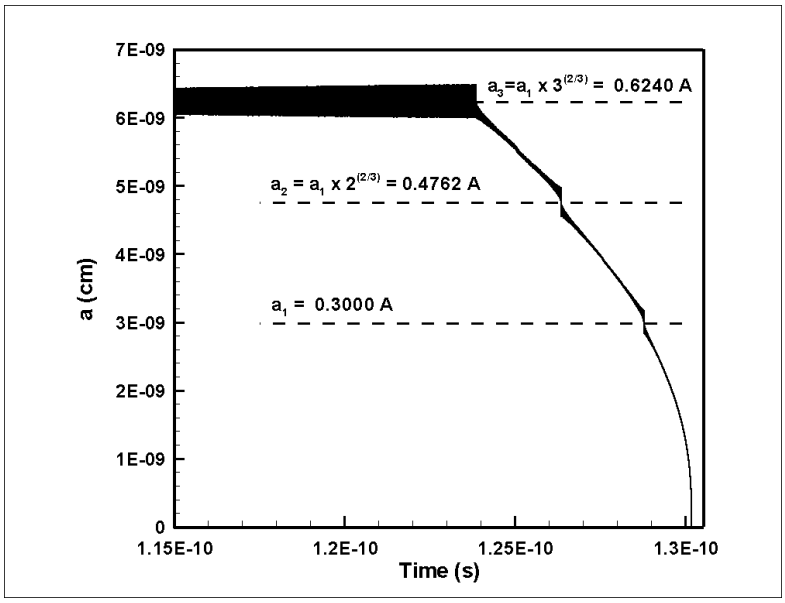

Fig. 2b Here, the $a\,(t)$ vs. t curve in Fig. 2a is examined closely at the region where the $n = 3$ subharmonic resonance changes to one of orbital decay. After the electron leaves the $n = 3$ subharmonic state, it past through two other resonant states, with conditions of A, ε, α, insufficient to delay decay at these points. These other resonant positions occurred at the $n = 2$ and $n = 1$ positions: $a_2 = a_1 \times 2^{2/3}\,\text{Å} = 0.4762\,\text{Å}$, and $a_1 = 0.3\,\text{Å}$. As in Fig. 2a, $A = 35,000$ statvolt/cm, $a_{\text{initial}} = 0.7\,\text{Å}$, and $\varepsilon_{\text{initial}} = 0$.

Figure 2c shows a blown up view of ε vs. t when the end of the $n = 3$ subharmonic resonance state is reached. As can be seen, $\varepsilon \approx 0.669$ when decay sets in. The value of 0.6706 is shown, which is the analytic value computed in Sec. IV, and close (good to three digits) to the simulated/computed value, although not as close as the $n = 2$ case shown in Sec. I, which agreed to four digits.

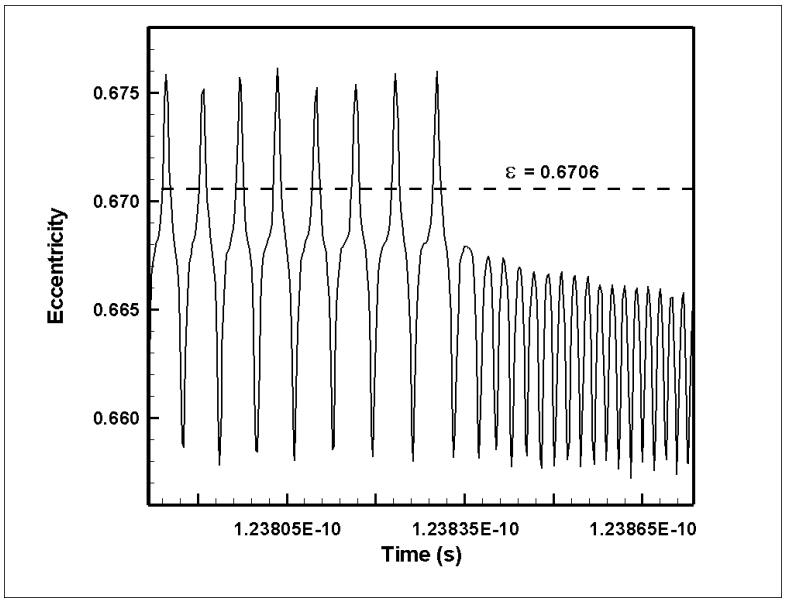

Fig. 2c This plot shows the behavior of ε vs. t at the point where the $n = 3$ resonance condition in Fig. 2a changes to orbital decay.

Figure 3 demonstrates the "universality" of $\varepsilon_{\mathrm{crit},n} \approx 0.554$ for the $n = 2$ subharmonic resonance, for the situation where the classical electron's orbit begins in a circular orbit with semimajor axis a greater than the $a_2 = a_1 2^{2/3}$ resonance point, and with the CP wave amplitude large enough to cause resonance once the orbit decays to a_2. Figures 3a and 3b concern the situation, where $a_1 = 0.5\,\text{Å}$, or the angular frequency of the CP wave is $\omega_1 = \left(\frac{e^2}{ma_1^3}\right)^{1/2} = 4.5011 \times 10^{16}\,\mathrm{s}^{-1}$. The starting radius is $0.9\,\text{Å}$, and six simulations are superimposed, each with a different CP wave amplitude: $A = 100$, 500, 1000, 5000, 10, 000, and 50, 000 statvolt/cm.

In Fig. 3a, a vs. t is shown. As can be seen, the electron is "caught" at $a_2 = a_1 2^{2/3} = 0.7937\,\text{Å}$ in all six cases. The length of time in the $n = 2$ subharmonic resonance varies, with the 500 statvolt/cm being the longest, then with decreasing times in the order of 1000, 5000, 10,000, 50,000, and 100 statvolt/cm. Similar situations were shown for the $n = 1$ case in Refs. [4] and [5]. The larger the value of A, the larger becomes the "envelope" of the a vs. t fluctuations around the $a_2 = 0.7937\,\text{Å}$ point, with the widest ending envelope here being the one with $A = 50,000$ statvolt/cm.

Figure 3b turns to examine these same simulations, but now plotting $\varepsilon\,(t)$ vs. t. In each case, ε starts at zero, since the initial orbit is circular, then increases until the value of $\varepsilon_{\mathrm{crit},2} \approx 0.554$, at which point the orbit goes back into decay, similar to Fig. 1d. The key point is that all have essentially the same value of $\varepsilon_{\mathrm{crit},2}$ for when the orbit changes from one of $n = 2$ subharmonic resonance to decay, of $\varepsilon = 0.554$ (Sec. V will cover related points).

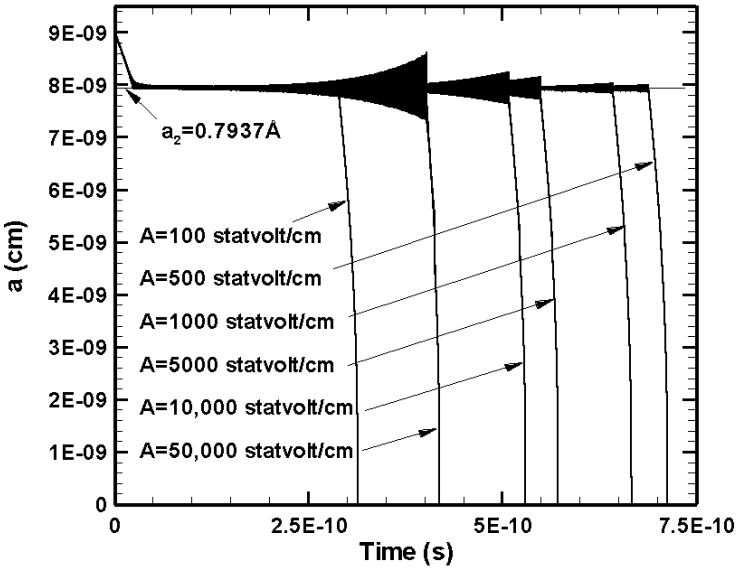

Fig. 3a Here a range of CP amplitude A values (100, 500, 1000, 5000, 10,000, and 50,000 statvolt/cm) are simulated for the conditions of the CP wave's angular velocity being $\omega_1 = \left(\frac{e^2}{ma_1^3}\right)^{1/2}$, with $a_1 = 0.5\,\text{Å}$. In each case the starting radius is $0.90\,\text{Å}$, with $\varepsilon_{\text{initial}} = 0$, $\alpha = 0$. The resonance encountered here is $n = 2$, $a_2 = a_1 2^{2/3} = 0.7937\,\text{Å}$. As can be seen, all situations have a strong resonance at this a_2 value, with the main difference being twofold: (1) the larger A is, the larger the envelope of oscillations of a about a_2; (2) A can clearly effect the duration time in this $n = 2$ subharmonic resonance.

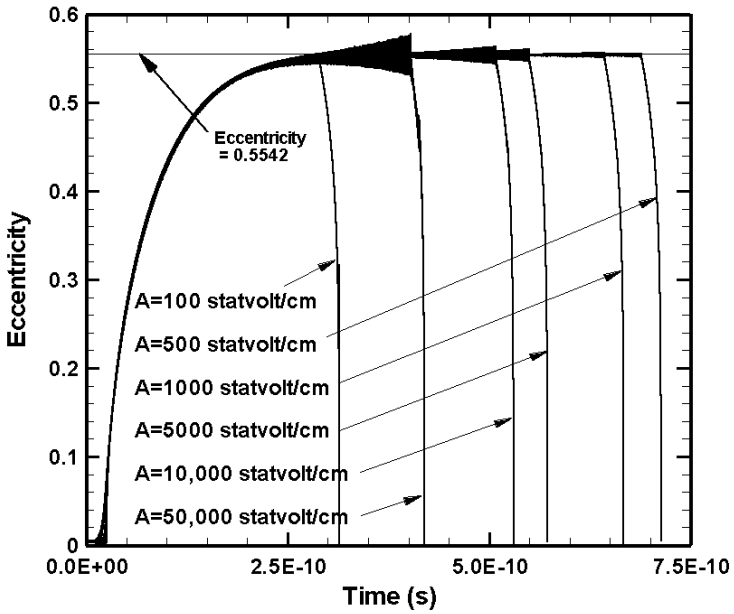

Fig. 3b The same simulation conditions as in Fig. 3a also here, but now ε vs. t is plotted for each of the six A values examined of 100, 500, 1000, 5000, 10,000, and 50,000 statvolt/cm. All curves show that $\varepsilon_{\mathrm{crit},2} \approx 0.5542$. This result occurred despite the difference of 500 factor difference in A values, from 100 to 50,000 statvolt/cm. Other behaviors differed, such as the envelope size of the fluctuations in ε, and the length of time in resonance, but $\varepsilon_{\mathrm{crit},2}$ was largely independent of A, much like a_2 was common for all the curves in Fig. 3a.

Originally, we intended to display several more sets of figures like 3a and 3b, each at different a_1. However, the same behavior is observed in each, so perhaps displaying all these plots is not necessary. Indeed, the following same behavior would have been seen for a wide range of a_1 values, namely, (1) the final eccentricity before decay is very close to 0.554, if not even closer to the the 0.5542 analytical value later calculated in Sec. IV; (2) the envelope around the a vs. t curve always increases in width as A increases; and (3) that the length of time of an $n = 2$ resonance certainly depends on the value of A, reaching a longest value (here it was for 500 statvolt/cm), then decreasing as A becomes larger beyond that point.

Incidentally, it is a curious point from a classical physics point of view, that circular orbits have a bit of "preference," or likelihood of occurrence, over orbits with $\varepsilon > 0$, for simple situations with either no radiation applied, or perhaps one CP wave applied. When a large range of radiation frequencies and amplitudes are applied, as in the stochastic situation of Ref. [6], then the following comment does not hold, but for simple situations as just mentioned, the radiation reaction term in the Lorentz-Dirac equation acts in such a way as to return an initially decaying elliptical orbit back toward a circular (decaying) orbit. This was noted in Ref. [3], Fig. 4, in particular, and also

in several points and figures later in [3] where various applied radiation conditions occurred. Here, we also see this point in Fig. 3b, where once the electron falls out of resonance, the radiation reaction term acts to make $\varepsilon \to 0$ as the orbit decays.

To help illustrate these behaviors further, Fig. 4 shows how r vs. t occurs for the $a_1 = 0.5\,\text{Å}$ case in Fig. 3. As the eccentricity starts to increase once subharmonic resonance is reached, the orbit changes from circular to elliptical character, with a minimum radius of $(1-\varepsilon)\,a$ and a maximum radius of $(1+\varepsilon)\,a$ in each orbit. At the point of onset of decay, with $a_2 = a_1 2^{2/3} = 0.7937\,\text{Å}$ and $\varepsilon_{\text{crit},n} \approx 0.554$, then $r_{\min} = 0.354\,\text{Å}$ and $r_{\max} = 1.234\,\text{Å}$, agreeing fairly nicely with the data shown in Fig. 4. Changing the CP amplitude A does not significantly alter the envelope of the huge number of orbit fluctuations in Fig. 6, nor does it influence the final value of $\varepsilon_{\text{crit},2}$, but it does alter the length of time that the subharmonic resonance lasts before decay sets in again.

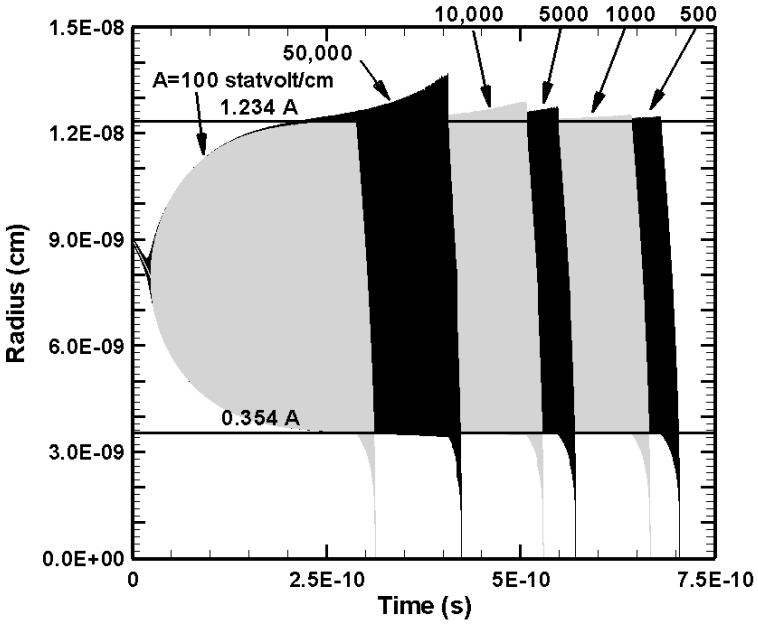

Fig. 4 This figure contains a set of plots that corresponds to Fig. 3, where $a_1 = 0.5\,\text{Å}$. The large radius change is due to the orbit, initially in a circular state, changing to an elliptical state, where the maximum of the eccentricity is about 0.554, and is largely independent of the value of the CP amplitude. The two horizontal lines of 1.234 Å and 0.353 Å represent the maximum and minimum of the radius, given that $\varepsilon_{\max} \approx 0.554$.

Finally, before turning to the next section involving an analytical analysis of $\varepsilon_{\text{crit},n}$, Fig. 5 shows a plot of θ_0 vs. t for the corresponding case of Fig. 1, where $a_1 = 0.6\,\text{Å}$ and $a_2 = a_1 2^{2/3} = 0.9524\,\text{Å}$. Here, θ_0 increases the most in the situation in Fig. 1 ($a_1 = 0.6\,\text{Å}$) when $A = 50,000$ statvolt/cm (of the six situations examined of 100, 500

1000, 5000, 10,000, 50,000 statvolt/cm), with about 57,000 radians change occurring for θ_0, when in subharmonic resonance. If we were to plot θ_0 for the case of Fig. 4 where $a_1 = 0.5\,\text{Å}$, we would see about 33,500 radians being the maximum when $A = 50,000$ statvolt/cm, and if we were to examine a yet smaller semimajor case, when $a_1 = 0.4\,\text{Å}$, then 17,000 radians would occur during resonance when $A = 50,000$ statvolt/cm.

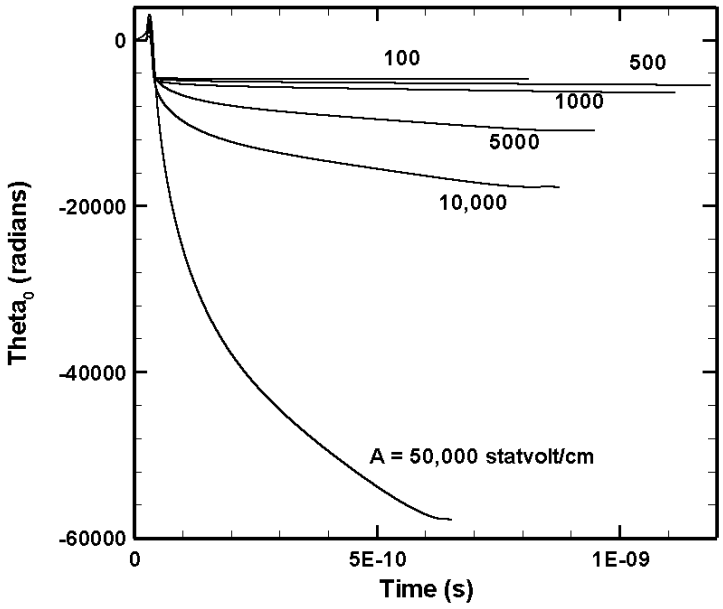

Fig. 5 Plot of θ_0 vs. t, for the situation in Fig. 3. Here, $a_1 = 0.6\,\text{Å}$. The larger the value of A, the more the elliptical orbit rotates while the classical electron is in the subharmonic resonance state.

4 Analysis of critical values of ε

To deduce the values of $\varepsilon_{\text{crit},n}$, we will start with the conserved quantities in the classic Kepler-Coulombic case of a central force with a $1/r^2$ dependence, which in our case means the situation where no CP plane wave acts and no radiation reaction exists. We will then examine how these otherwise conserved quantities, change with time due to the CP wave and the radiation reaction. The natural conservation quantities to consider are the energy, the angular momentum vector, and the Laplace-Runge-Lenz vector. As discussed in [22], the angular momentum vector and the energy alone contain only four independent constants of the motion, while the Laplace-Runge-Lenz vector adds one more. We will make use of this work, nicely presented in texts such as [22] and [23]. We make the approximation that the orbit remains essentially in a two dimensional plane during the duration of the resonance and the subsequent decay and that the natural Coulombic based orbit is slowly modified by the additional forces of the CP plane wave and the small, but constant, radiation reaction. Identifying the

normally constant Coulombic parameters and having them slowly change due to these additional forces, will be sufficient to deduce much about $\varepsilon_{\mathrm{crit},n}$.

Multiplying (12) by the radial speed $\dot{r}$, and multiplying (13) by the speed $r\dot{\theta}$ in the increasing θ direction, adding the two contributions, then yields, after a bit of manipulation:

$$\begin{aligned} &\frac{d}{dt}\left[\frac{m}{2}\left(\dot{r}^2+r^2\dot{\theta}^2\right)-\frac{e^2}{r}\right] \\ &=\tau e^2\left(2\frac{\dot{r}^2}{r^3}-\frac{\dot{\theta}^2}{r}\right)+eA\left[\dot{r}\sin\left(\theta-\omega_1 t-\alpha\right)+r\dot{\theta}\cos\left(\theta-\omega_1 t-\alpha\right)\right] \quad . \end{aligned} \tag{19}$$

The left side is the time rate of change of the kinetic energy, in polar coordinates, plus the time rate of change of the Coulombic potential energy. On the right side, the first term is the nonrelativistic rate of work by the radiation reaction term, very weak, but always present and causing the tendency for orbital decay. The second term on the right is the rate of work by the Lorentz force of the CP wave acting on the classical electron, normally varying rapidly in sign, but with a sign correlation occurring when orbital angular frequency and applied frequency ω_1 match up. If the radiation reaction and CP wave did not exist, then the left side would equal zero, and the kinetic plus Coulombic potential energy would be a constant.

Similarly, the angular momentum rate equation can be deduced by multiplying (13) by r and converting it into:

$$\frac{d}{dt}\left(mr^2\dot{\theta}\right)=-\frac{\tau e^2\dot{\theta}}{r}+erA\cos\left(\theta-\omega_1 t-\alpha\right) \quad . \tag{20}$$

The left side is the time rate of change of $L_z = mr^2\dot{\theta}$, the angular momentum component perpendicular to the plane of the orbit, written in polar coordinates. On the right side, the first term is the nonrelativistic torque expression due to the radiation reaction, again, very weak, but always present. The second term on the right is the torque acting on the orbiting classical electron due to the Lorentz force of the CP wave. If the radiation reaction and CP wave were not present, L_z would be a constant.

Following standard treatments such as in [22], [23], [24], when the right sides of (19) and (20) equal zero, corresponding to the pure Kepler-Coulombic problem of (3), then for a bound orbit,

$$\dot{\theta}=\frac{e\left[1-\varepsilon\cos\left(\theta-\theta_0\right)\right]^2}{m^{1/2}a^{3/2}\left(1-\varepsilon^2\right)^{3/2}} \quad , \tag{21}$$

and from (14) and (21)

$$L_z=mr^2\dot{\theta}=e\left(am\right)^{1/2}\left(1-\varepsilon^2\right)^{1/2} \quad , \tag{22}$$

where the approximation sign would be replaced by an equality sign if radiation damping and the CP wave were not present.

Assuming the rate of time variation in a, ε, and θ_0 is small, compared to the much more rapid time variation in $\theta\left(t\right)$, then also from (14) and (21), one can show that

$$\frac{m}{2}\left(\dot{r}^2+r^2\dot{\theta}^2\right)-\frac{e^2}{r}\approx-\frac{e^2}{2a} \quad . \tag{23}$$

From (19) and (23),

$$\frac{d}{dt}\left(-\frac{e^2}{2a}\right) \approx \tau e^2\left(2\frac{\dot{r}^2}{r^3}-\frac{\dot{\theta}^2}{r}\right) + eA\left[\dot{r}\sin\left(\theta-\omega_1 t-\alpha\right)+r\dot{\theta}\cos\left(\theta-\omega_1 t-\alpha\right)\right] \quad , \tag{24}$$

and from (20) and (22),

$$\frac{d}{dt}\left[e\left(am\right)^{1/2}\left(1-\varepsilon^2\right)^{1/2}\right] \approx -\frac{\tau e^2\dot{\theta}}{r}+erA\cos\left(\theta-\omega_1 t-\alpha\right) \quad . \tag{25}$$

The simulations reported in this article arise from numerically solving for $r\left(t\right)$ and $\theta\left(t\right)$ in (12) and (13), while the fitted parameters a, ε, and θ_0 to these orbits come from the least squares fit method discussed in Sec. II. Equations (24) and (25) contain a mixture of these variables and were deduced to enable an understanding of the interesting values of $\varepsilon_{\mathrm{crit},n}$ that result when orbits in a subharmonic state eventually fall out of resonance and turn back into decaying orbital paths.

To ensure that the approximations make sense, Fig. 6 offers some insight into the approximations by comparing the situation for the exact same conditions of Fig. 1 in Sec. 1. As observed in Fig. 6, the plots of $E=\frac{1}{2}m\mathbf{v}^2-\frac{e^3}{r}$ versus the approximate value of $-\frac{e^2}{2a}$, and $L_z=mr^2\dot{\theta}$ versus the approximate value of $e\left(am\right)^{1/2}\left(1-\varepsilon^2\right)^{1/2}$, works quite well for this situation, and helps to justify the above analysis.

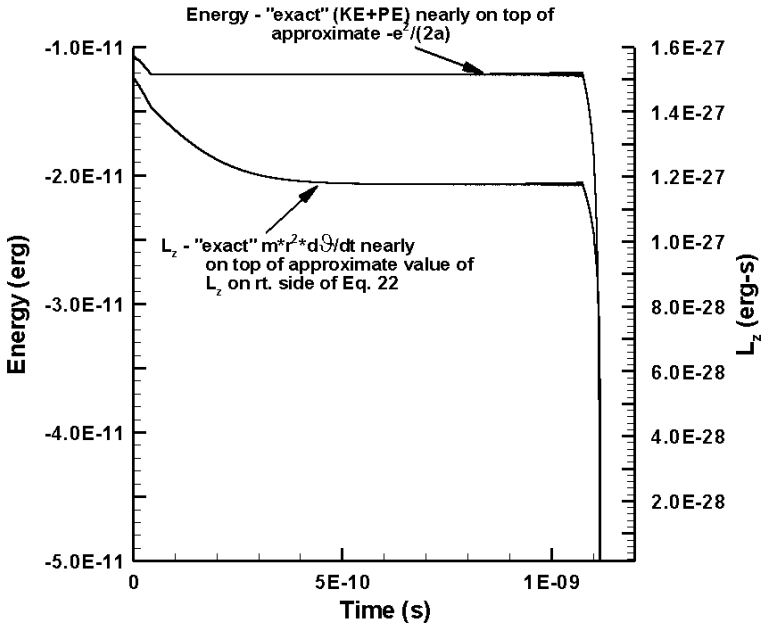

Fig. 6a There are four curves here. The top two involving energy, are essentially on top of each other. Likewise, the bottom two involving angular momentum, are essentially indistinguishable at this view. The top two curves are $E=\frac{1}{2}m\mathbf{v}^2-\frac{e^3}{r}$

and the approximate value $-\frac{e^2}{2a}$. The bottom two are $L_z = mr^2\dot{\theta}$ and the approximate value $e\,(am)^{1/2}\left(1-\varepsilon^2\right)^{1/2}$. The conditions for the simulation are the same as in Fig. 1, namely, $a_1 = 0.6\,\text{Å}$, $\omega_1 = \left(\frac{e^2}{ma_1^3}\right)^{1/2}$, the orbit began at $a = 1.08\,\text{Å}$ in a circular orbit, so $\varepsilon_{\text{initial}} = 0$, $A = 1000$ statvolt/cm, and $a_2 = a_1 2^{2/3} \approx 0.9524\,\text{Å}$, and $\alpha = 0$.

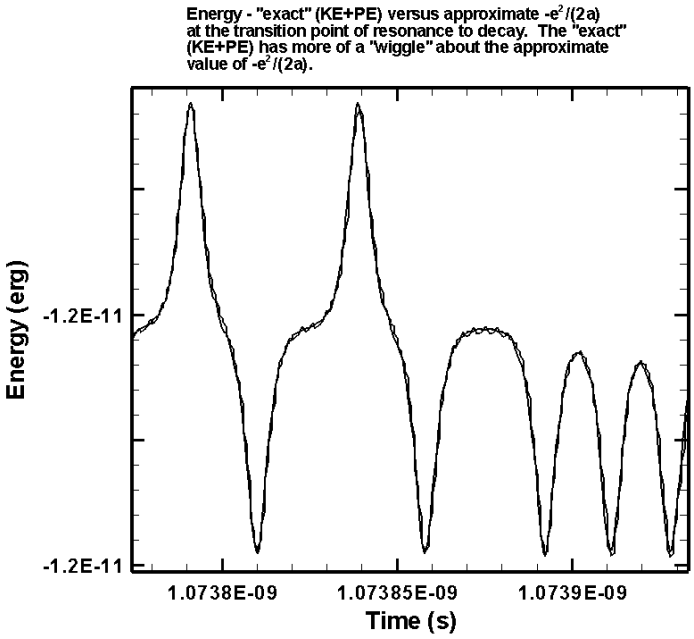

Fig. 6b This plot "zooms" in on the transition point between subharmonic resonance and orbital decay in the top two curves in Fig. 8a, around $t \approx 1.07385 \times 10^{-9}\,\text{s}$. The two curves are $E = \frac{1}{2}m\mathbf{v}^2 - \frac{e^3}{r}$ and $-\frac{e^2}{2a}$, with the former curve of $\frac{1}{2}m\mathbf{v}^2 - \frac{e^3}{r}$ vs. t having the more "wiggles," for lack of a better description. Clearly, the two curves match each other quite well.

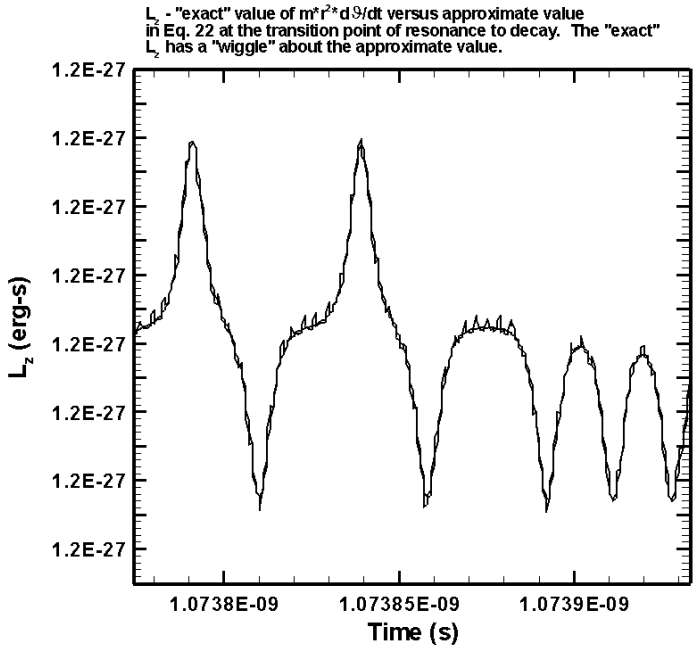

Fig. 6c This plot also "zooms" in on the transition point between subharmonic resonance and orbital decay in the top two curves in Fig. 4a, around $t \approx 1.07385 \times 10^{-9}$ s. The two curves are $L_z = mr^2\dot{\theta}$ and $e\,(am)^{1/2}\left(1-\varepsilon^2\right)^{1/2}$, with the former curve of $mr^2\dot{\theta}$ vs. t having the more "wiggles." Clearly, the two curves match each other quite well.

To make further progress on deducing the $\varepsilon_{\mathrm{crit},n}$values, we first note that when in resonance, $a \approx$ constant; hence, the kinetic plus potential energy (23), which is approximately $-\frac{e^2}{2a}$, is therefore also approximately constant. Now, this isn't exactly true, as a is certainly fluctuating when in resonance, and the fluctuation grows over time, as evident from Fig. 3a; this fact we will need to take into account. This will be done by taking a short time average,

$$\langle \quad \rangle \equiv \frac{1}{\tau}\int_{t}^{t+\tau} (\quad)\,dt' \quad ,$$

where the interval τ is sufficiently large to contain many oscillations of the quantities of interest, as in Fig. 2c, but not so large as to miss the key features, such as the start and end of resonance; i.e., we anticipate usually hundreds to thousands of orbits, then some of these difficulties can be avoided, and thereby pertain closer to the idea of a, ε, and θ_0 in the first place, since these parameters are intended to model the relatively slow evolution of the orbit.

Taking this time average over both sides in (24) during resonance, then the left side of (24) reduces to essentially zero. Physically, this is equivalent to saying that the time average of the first term on the right, which is negative, and in classical physics due to

electromagnetic energy being radiated off, is compensated by the positive energy, on average, that is pumped back into the orbit by the CP wave.

Taking a similar time average for (25) also helps. However, the left side does not always equal zero when in resonance as can be seen in Fig. 6a. The orbit becomes more and more elliptical throughout the evolution of the subharmonic resonance, so ε increases on average, with small oscillations superimposed. However, when ε reaches its maximum, as in Figs. 1d and 3b, then the time rate of change of $\langle\varepsilon\rangle$ is essentially zero. This is the point we are interested in, as this involves the value of $\varepsilon_{\mathrm{crit},n}$.

Physically speaking, the time average of the first term on the right in 25 provides a fairly constant acting torque that decreases the orbital angular momentum. The time average of the second term on the right averages over a stronger, but rapidly varying torque, between positive and negative values, from the CP wave. $\langle L_z\rangle$ decreases while in resonance, as in Fig. 6a, eventually arriving at a minimum, which is when orbital decay again sets in. At this point, the CP wave is no longer able to continue to stay in phase on average, particularly in terms of providing a positive average energy to counteract the small but constant radiation reaction. At this point $\langle L_z\rangle$ flattens out, which is where decay sets in, and is where $\left\langle \frac{d}{dt}L_z \right\rangle \approx 0$.

In Sec. V, we will come back to this last point of $\left\langle \frac{d}{dt}L_z \right\rangle \approx 0$, when the orbit changes from one of resonance to one of decay. This point turns out to not always be true. It is true for the simulation examples shown so far in this article, where the classical electron was started in a circular orbit with a either slightly larger, or a fair bit larger, than the n subharmonic resonance point of a_n. However, starting right near a_n, leads to a bit of an error in this conclusion. Again, we will return to this point in Sec. V.

Otherwise, by taking the time average of (24) and (25), setting the left sides to zero near the onset of orbital decay, and taking the ratio of the resulting nonzero terms, we obtain:

$$\frac{\left\langle \frac{\tau e^2 \dot{\theta}}{r} \right\rangle}{\left\langle \tau \frac{e^2}{r^3}\left[2\dot{r}^2 - \left(r\dot{\theta}\right)^2\right] \right\rangle} \approx -\frac{\langle erA\cos\left(\theta-\omega_1 t-\alpha\right)\rangle}{\left\langle eA\left[\dot{r}\sin\left(\theta-\omega_1 t-\alpha\right)+r\dot{\theta}\cos\left(\theta-\omega_1 t-\alpha\right)\right]\right\rangle} \quad . \tag{26}$$

An immediate satisfactory feature of this expression for deducing $\varepsilon_{\mathrm{crit},n}$, is that A cancels out on the right, as expected from Fig. 3b. Also, the τe^2 term cancels on the left, and e cancels on the right.

In the denominator on the right,

$$\begin{aligned} &\dot{r}\sin\left(\theta-\omega_1 t-\alpha\right)+r\dot{\theta}\cos\left(\theta-\omega_1 t-\alpha\right) \\ &= \frac{d}{dt}\left[r\sin\left(\theta-\omega_1 t-\alpha\right)\right]+r\omega_1\cos\left(\theta-\omega_1 t-\alpha\right) \end{aligned} \tag{27}$$

Upon taking the time average,

$$\begin{aligned} &\left\langle \frac{d}{dt}\left[r\sin\left(\theta-\omega_1 t-\alpha\right)\right] \right\rangle \\ &= \frac{1}{\tau}\int_t^{t+\tau} \frac{d}{dt'}\left[r\sin\left(\theta-\omega_1 t'-\alpha\right)\right] dt' \\ &= \frac{1}{\tau}\left\{r\left(t+\tau\right)\sin\left[\theta\left(t+\tau\right)-\omega_1\left(t+\tau\right)-\alpha\right]-r\left(t\right)\sin\left[\theta\left(t\right)-\omega_1 t-\alpha\right]\right\} \quad . \end{aligned} \tag{28}$$

Since r is bounded, then for a value of τ that is much larger than the period of an orbit, and encompasses a number of the fluctuations in a and ε, as in Figs. 1c, 1e, 2c, and as in evidence in 6b and 6c, then (28) becomes negligible compared to the time average of the remaining term on the right in (27). Hence,

$$\left\langle \dot{r}\sin\left(\theta-\omega_1 t-\alpha\right)+r\dot{\theta}\cos\left(\theta-\omega_1 t-\alpha\right)\right\rangle \approx \omega_1\left\langle r\cos\left(\theta-\omega_1 t-\alpha\right)\right\rangle \quad , \tag{29}$$

and the right side of (26) then simplifies enormously to simply being $-\frac{1}{\omega_1}$.

Working on the left side of (26) now,

$$\begin{aligned}\left\langle \frac{\dot{\theta}}{r}\right\rangle &= \frac{1}{\tau}\int_{t}^{t+\tau} dt'\,\frac{d\theta}{dt'}\frac{1}{r} = \frac{1}{\tau}\int_{\theta(t)}^{\theta(t+\tau)}\frac{d\theta}{r}\\ &= \frac{1}{\tau}\int_{\theta(t)}^{\theta(t+\tau)}\frac{\left[1-\varepsilon\cos\left(\theta-\theta_0\right)\right]}{a\left(1-\varepsilon^2\right)}d\theta \quad .\end{aligned} \tag{30}$$

As shown in the simulation figures, a and ε do have a small fluctuation about their center value when in resonance, but if we take their center values along the curves, and recognize the true source of rapid fluctuations, namely $\cos\left(\theta-\theta_0\right)$, which fluctuates with every orbit, while a, ε, and θ_0 vary over tens to hundreds of orbits, and if τ is made equal to $N\times T$, where T is the orbital period and N is of the order of perhaps 100, then the second term in the numerator contributes negligibly with larger N. The first term, however, without the large fluctuation on every orbit, can be evaluated via,

$$\frac{1}{\tau}\left[\theta\left(t+\tau\right)-\theta\left(t\right)\right] \approx \frac{1}{\left(N\times T\right)}2\pi N = \frac{2\pi}{T} \quad , \tag{31}$$

which does not diminish as N grows, resulting in the reasonable approximation of

$$\left\langle \frac{\dot{\theta}}{r}\right\rangle \approx \frac{2\pi}{Ta\left(1-\varepsilon^2\right)} \quad . \tag{32}$$

Here, a and ε are the central values over which the short time interval during which the average of $\frac{\dot{\theta}}{r}$ was taken, and T is the period of the orbit.

Finally for the denominator on the left in (26), first we note that

$$\dot{r} \approx \dot{\theta}\frac{d}{d\theta}\left[\frac{a\left(1-\varepsilon^2\right)}{1-\varepsilon\cos\left(\theta-\theta_0\right)}\right] = -\frac{e\varepsilon\sin\left(\theta-\theta_0\right)}{m^{1/2}a^{1/2}\left(1-\varepsilon^2\right)^{1/2}} \quad , \tag{33}$$

ignoring the small fluctuations in a, ε, and θ_0 here and using (21). Then,

$$\begin{aligned}
&\left\langle \frac{2\dot{r}^2 - \left(r\dot{\theta}\right)^2}{r^3} \right\rangle \\
&= \frac{1}{\tau} \int_{\theta(t)}^{\theta(t+\tau)} \frac{d\theta}{\dot{\theta}} \frac{\left[2\dot{r}^2 - \left(r\dot{\theta}\right)^2\right]}{r^3} \\
&\approx \frac{1}{\tau} \int_{\theta(t)}^{\theta(t+\tau)} \frac{d\theta}{\left\{\frac{e[1-\varepsilon\cos(\theta-\theta_0)]^2}{m^{1/2}a^{3/2}(1-\varepsilon^2)^{3/2}}\right\}} \frac{\left\{2\left[-\frac{e\varepsilon\sin(\theta-\theta_0)}{m^{1/2}a^{1/2}(1-\varepsilon^2)^{1/2}}\right]^2 - \left[\frac{e[1-\varepsilon\cos(\theta-\theta_0)]}{m^{1/2}a^{1/2}(1-\varepsilon^2)^{1/2}}\right]^2\right\}}{\left[\frac{a(1-\varepsilon^2)}{1-\varepsilon\cos(\theta-\theta_0)}\right]^3} \\
&= \frac{e}{a^{5/2}m^{1/2}\left(1-\varepsilon^2\right)^{5/2}} \frac{1}{\tau} \int_{\theta(t)}^{\theta(t+\tau)} d\theta \left(-1 + 3C\varepsilon - 3C^2\varepsilon^2 + 2S^2\varepsilon^2 + C^3\varepsilon^3 - 2CS^2\varepsilon^3\right) \qquad (34)
\end{aligned}$$

where $\cos(\theta - \theta_0)$ and $\sin(\theta - \theta_0)$ were abbreviated by C and S in the last line.

Again treating that ε and θ_0 vary insignificantly during τ, at least as compared with $\theta(t)$, then there are only three terms in the integrand that do not fluctuate between negative and positive, namely, -1, $-3C^2\varepsilon^2$, and $+2S^2\varepsilon^2$. The remaining terms after being integrated over and divided by τ, will be negligible. Thus, again for N of the order of 100 or more orbital periods,

$$\begin{aligned}
&\frac{1}{\tau} \int_{\theta(t)}^{\theta(t+\tau)} d\theta \left(-1 + 3C\varepsilon - 3C^2\varepsilon^2 + 2S^2\varepsilon^2 + C^3\varepsilon^3 - 2CS^2\varepsilon^3\right) \\
&\to \frac{1}{NT} \int_{\theta(t)}^{\theta(t)+N2\pi} d\theta \left(-1 - 3C^2\varepsilon^2 + 2S^2\varepsilon^2\right) \\
&= \frac{1}{NT}\left(-N2\pi - 3N\pi\varepsilon^2 + 2N\pi\varepsilon^2\right) = \frac{1}{T}\left(-2\pi - \pi\varepsilon^2\right) \quad . \qquad (35)
\end{aligned}$$

The result is

$$\left\langle \frac{2\dot{r}^2 - \left(r\dot{\theta}\right)^2}{r^3} \right\rangle \approx -\frac{e\pi\left(2+\varepsilon^2\right)}{a^{5/2}m^{1/2}\left(1-\varepsilon^2\right)^{5/2}T} \quad . \qquad (36)$$

Combining the numerator and denominator on the left side of (26), noting that T cancels out, and equating to our result on the right of $-\frac{1}{\omega_1}$,

$$\frac{\frac{2\pi}{a(1-\varepsilon^2)}}{-\left[\frac{e\pi(2+\varepsilon^2)}{a^{5/2}m^{1/2}(1-\varepsilon^2)^{5/2}}\right]} = -\frac{1}{\omega_1} \quad . \qquad (37)$$

Finally, the relation between the $n = 1$ period T_1 due to the CP wave ω_1, and the period T_n of the n^{th} order subharmonic orbit, is $T_n = nT_1$, so the period for the $n = 2$ subharmonic resonance orbital is twice the period of the CP wave, etc. Moreover, for a classical electron in an elliptical orbit with semimajor axis a (Kepler-Coulomb result),

$$T = \frac{2\pi}{\left(\frac{e^2}{ma^3}\right)^{1/2}} \quad , \qquad (38)$$

so that

$$\omega_1 = \frac{2\pi}{T_1} = \frac{2\pi n}{T_n} = n\left(\frac{e^2}{ma_n^3}\right)^{1/2} \quad , \tag{39}$$

where a_n is the semimajor axis of the orbit while in the n^{th} subharmonic resonance.

Combining, (37) reduces to

$$n = \frac{\left(2+\varepsilon_{\text{crit},n}^2\right)}{2\left(1-\varepsilon_{\text{crit},n}^2\right)^{3/2}} \quad . \tag{40}$$

The label $\varepsilon_{\text{crit},n}$ was inserted here since this was deduced at the peak of the eccentricity curve, when $\left\langle \frac{d}{dt}\left[e\,(am)^{1/2}\left(1-\varepsilon^2\right)^{1/2}\right]\right\rangle \approx 0$ in (25). Here, $n = 2, 3, ...$, and further examples will be provided in the next section that confirm the above result.

Numerically solving for $\varepsilon_{\text{crit},n}$ in (40) for a number of values of n in (40), Table 1 lists the first set of values of $\varepsilon_{\text{crit},n}$ for $n = 2, 3, ..., 7$. Figure 9 plots these values of $\varepsilon_{\text{crit},n}$ up through $n = 20$, assuming that the orbit can be caught into a subharmonic resonance state. As can be seen for the $n = 2$ and 3 subharmonic resonance cases shown in Figs. 1 and 2, respectively, the first two values in Table 1 agree to three (Fig. 2) or four (Fig. 1) decimal places of the earlier simulation examples.

n	$\varepsilon_{\text{crit},n}$
2	0.5542
3	0.6706
4	0.7316
5	0.7703
6	0.7975
7	0.8178

Table 1: $\varepsilon_{\text{crit},n}$ calculated for the first six (2, 3, ...,7) subharmonic resonances, assuming the orbit can be "caught", starting with a circular orbit.

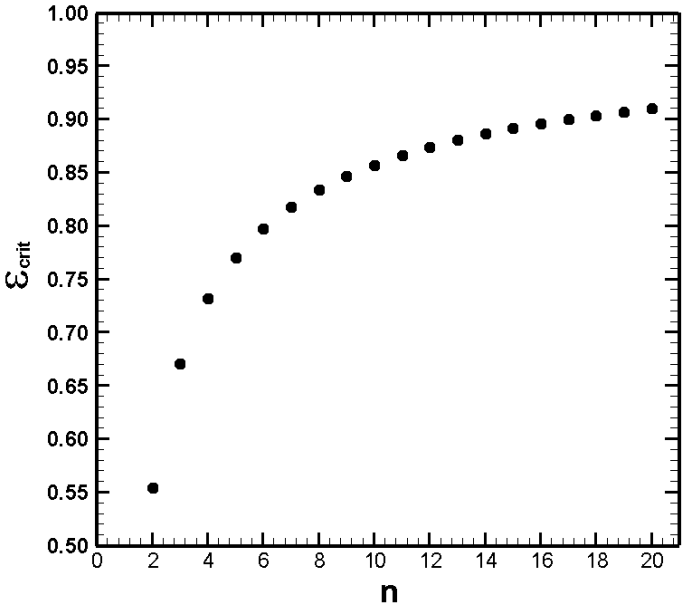

Fig. 7: Plot of $\varepsilon_{\mathrm{crit},n}$ vs. n, where n represents the subharmonic resonance level. The first six values are in Table 1.

5 Physical insight into resonance behavior, and caveats on this work

The analysis in the previous section works reasonably well. Here we briefly comment on some of the physical insights regarding these resonances. In addition a number of caveats will be discussed, including some subtle and qualitative points.

To start, the $n = 1$ resonances discussed in some detail in [2]-[5], have many interesting properties and similarities to the subharmonic resonance examples covered here ($n = 2, 3, ...$). The $n = 1$ resonances can have fairly long resonance times, and are effected by A and α in interesting ways. However, as not discussed in earlier work, $n = 1$ resonances seem very "poor" at "catching" an electron, meaning, if an orbit decays into an $n = 1$ resonance position, rarely are the conditions such that the orbit turns into a long lasting resonance state. Indeed, the long lasting $n = 1$ states analyzed in [2], [4], and [5] were created with the orbit starting essentially already in the $n = 1$ state.

In contrast, the $n = 2$ and 3 cases are "generally quite good" at catching the electron, providing that A is above a critical value. However, for $n \geq 4$, the "poor catching" situation again arises; indeed, it was nontrivial to come up with examples for this article where such events can happen. Nevertheless, three examples were obtained for $n = 4, 5, 6$, but they were not obtained from an initial circular $\varepsilon \approx 0$ start.

Note that when the electron's orbit decays into and past a subharmonic resonance point, even though it may not be "caught" for a relatively long duration, the "sign" or "presence" of the resonance is nearly always observable, as in the "blips" of a vs. t

in Fig. 2b and the soon to be discussed Fig. 8b. Indeed, if one "zooms" into the small resonance regions, such signatures can be seen in nearly all such plots of the relevant physical properties such as a, b, ε, E, and L_z, versus t.

Regarding what enables "capture," the key parameters are certainly: (1) A, as this ultimately dictates how much energy can be pumped into the orbit to offset the constant, but small, energy lose due to radiation reaction; (2) the phase difference α between the initial velocity vector and the CP electric field; and (3) the initial ε of the orbit as it nears or enters the resonance. However, except for this simple listing of parameters, the key factor comes back to $\mathbf{F} \cdot \mathbf{v}$ vs. t, where $\mathbf{F}$ is the sum of the Lorentz force due to electromagnetic radiation, and the largely resistive, but weak, radiation reaction force. Figure 1f gave an example of this behavior at the point when the orbit changed from one of resonance to decay. The behavior of this plot largely dictates the conditions and behavior of resonance, in a statistical sense involving the correlation in time of $\mathbf{F}$ and $\mathbf{v}$.

As mentioned earlier, the $n \geq 2$ situations are typically many times more complicated than the $n = 1$ case. For $n = 1$, the "applied CP force" is roughly in "sync" or out of sync for tens to hundreds of orbits, leading to plots like Fig. 5 in [2] and Fig. 3 in [4]. In contrast, for $n \geq 2$, the CP electric field is in and out of sync with $\mathbf{v}\,(t)$ roughly by a factor of n during every orbit. At first blush, there should be some surprise that there is any resonance at all for $n \geq 2$, but there is, and in certain cases, such as $n = 2$ and 3, the resonance is quite significant, of long duration, and able to "catch" decaying orbits under a variety of conditions. Ultimately, it comes down to a statistical analysis averaging over the "energy in" and "energy out" periods, with the former being larger during resonances, before final decay begins. Such predictive calculations are not easy to deduce, and hence the large reliance on simulation here.

Possibly why the $n = 3$ and 4 subharmonic resonances more easily catch a decaying orbit, than the $n = 1$, is that the $n = 2$ and 3 situations (Fig. 1f) provide rapid plus and minus power contributions in every orbit. If the phase is not quite right, over a series of such fluctuations, one or more will eventually provide the right input power to put the orbit on a resonance path. In contrast, for the case of $n = 1$, the scenario is quite different, as positive and negative power inputs to the orbit last over tens to hundreds of orbits. However, this is just a qualitative idea and there clearly is more to be tested and examined here to better understand the situation in more detail. Two key pieces here are that (1) the orbit is altered by the CP wave, and the (2) CP force and electron velocity must be in sync, at least on average, for a net power input to be created to compensate the radiation reaction effects.

Turning to more "caveats" and qualitative points, first, the analytical/numerical results of Table 1 and Fig. 7 do seem to reasonably hold, but there are problems beyond $n \geq 4$. We illustrate that they can certainly happen, as shown in Figs. 8a,b,c,d. Figure 8a shows catching the electron in an $n = 4$ state. The center of the eccentricity curve is good through the first two digits of the predicted value from Table 1 (*i.e.*, $\varepsilon_{\mathrm{crit},4} \approx 0.73$), but not better, which is a bit interesting since the $n = 5$ case was similar, but the $n = 6$ comes closer, and certainly the opening $n = 2$ example in Sec. I was far better. We will shortly be able to explain part of this reason as being due to the starting point of a in the simulation.

Figure 8b focuses on the point of decay in Fig. 8a. a vs. t is plotted in this narrow time region, showing that as the electron decays, a net of four, very clear subharmonic resonances are passed through. The values of $a_n = a_1 n^{2/3}$ are extremely precise.

Here, as in most cases, only one clear "catch" is made (*i.e.*, at $n = 4$, but not at the subsequent $n = 3$, 2, or 1 resonance points).

The other interesting feature of Fig. 8b, is that additional small signs of resonances can be observed that have not been discussed yet. In terms of the a vs. t curve, these are far less noticeable than the ω_1/n subharmonic resonances discussed in this article. Their values are midway between the subharmonic resonances with periods T_1 times $1, 2, 3, 4$ ($T_1 = \frac{2\pi}{\omega_1}$ is the CP wave period), and have precise values T_1 times $\frac{3}{2}$, $\frac{5}{2}$, and $\frac{7}{2}$. Such resonances of the type $\frac{n}{m}\omega_1$, where n and m are integers, have been studied for one dimensional oscillators. Here we see their presence, but clearly their effect on the orbit is small compared to the ω_1/n resonances.

Figure 8c shows a case where a decaying electron orbit is caught in a $n = 5$ subharmonic resonance, while Fig. 8d shows a similar case for $n = 6$. The "caveats" to mention here is that none of these examples of $n = 4, 5, 6$ "catches in Fig. 8, were easy to come by. As mentioned earlier, resonance signs of "blips" in an a vs. t decaying curve are easy to spot, such as in Fig. 2b or 8b, and can be obtained for high numbers like $n = 10$, and higher. However, it appears nontrivial for $n \geq 4$ to obtain conditions such that the electron doesn't just decay through the resonance, but rather hangs for a substantial time at a_n. Evidently, the higher the value of n, to some extent the harder it is to find the right condition.

For $n = 2$ or 3, the key concern seems to be to make A larger than some critical value, as discussed in [1]. For the $n = 4$ case here, besides the value of A (here 75,000 statvolt/cm), the initial eccentricity had to be about 0.05, and the electron had to start very close to a_4. For the $n = 5$ case in Fig. 8c, the initial value of ε had to be increased to 0.1 before the "catch" was accomplished. The same was true for the $n = 6$ case in Fig. 10d, but here the electron needed to be "dropped" at a slight "height" above a_6 before the "catch" could be accomplished. Indeed, starting at $a_6 = 0.25 \times 6^{2/3}\,\text{Å} = 0.8255\,\text{Å}$, resulted in the electron not being caught at the $n = 6$ point, nor at the next $n = 5$, 4, and 3 resonance points, but decayed right past all of these before finally being caught at $n = 2$. The resonance "blips" were observable, but the conditions were not such as to make the "catch." Changing the starting a value just slightly, from $a_6 = 0.8255\,\text{Å}$ to $0.83\,\text{Å}$, however, enabled the $n = 6$ catch shown in Fig. 8d.

This article does not address why such slight changes can have such large effects. Physically speaking, the reason is certainly clear, as the answer goes back to Fig. 1f concerning $\mathbf{F} \cdot \mathbf{v}$ vs. t. When the CP wave can provide a positive energy input to the trajectory, on average, over many orbits, then the decaying effect of the constantly acting radiation reaction can be compensated. $\mathbf{F} \cdot \mathbf{v}$ alters the orbit in subtle ways, providing a statistical impact of positive and negative energy input. A positive correlation effect between $\mathbf{F}$ and $\mathbf{v}$ can keep the orbit in a somewhat stable resonance state. Predicting precise effects from A, initial a, initial ε, and α, has apparently greater sensitivity for higher values of n.

Thus, some mention and examples have been provided of the often subtle, but important impact on obtaining sustained subharmonic resonances due to different values of A, initial a, initial ε, and α. Regarding α, the angle between $-e\mathbf{E}_{\text{CP}}$ and $\frac{d}{dt}\mathbf{z}$ at $t = 0$, we have not discussed its effect much yet, but it can have a fair impact on the length of time that the semi-stable resonances lasts, as covered in some detail in [5] for $n = 1$. Not surprisingly, for $n \geq 2$ resonances, similar effects occur, as α can effect how long correlation can exist between the electron's motion and the CP wave.

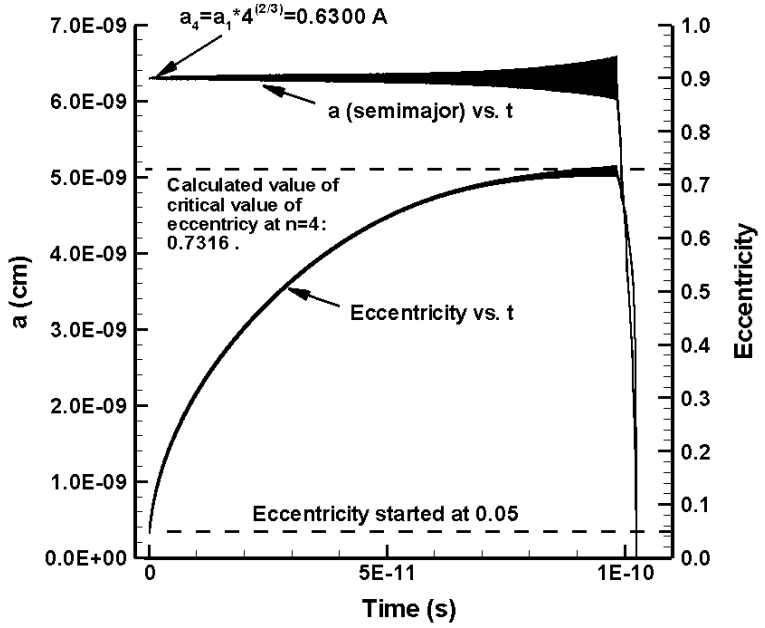

Fig. 8a Here the classical electron was "caught" in an $n = 4$ subharmonic resonance state. $a = 0.25\,\text{Å}$, $a_4 = a_1 4^{2/3} = 0.6300\,\text{Å}$. $A = 75,000$ statvolt/cm, $\alpha = 0$, $\varepsilon_{\text{initial}} = 0.05$, $a_{\text{initial}} = a_4$. The simulation value of $\varepsilon_{\text{crit},4}$ agreed to the first two digits of the analytically computed value in Table 1 of 0.7316.

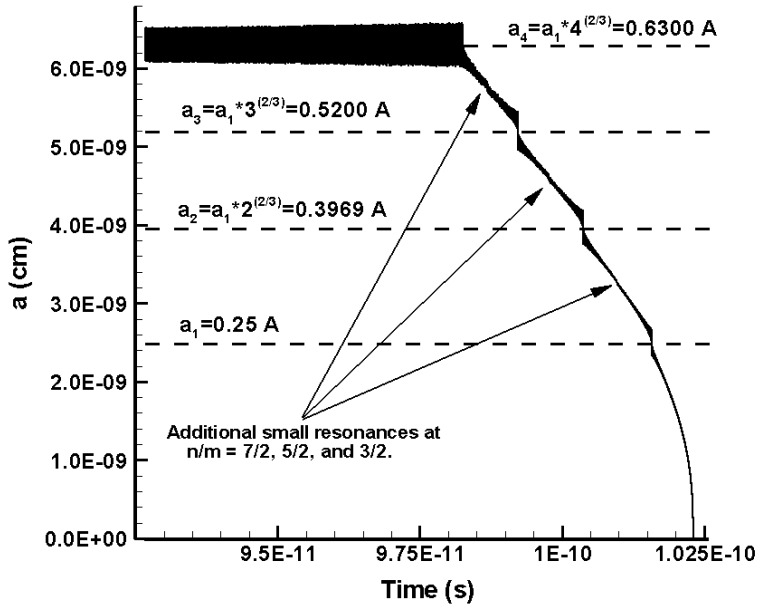

Fig. 8b Here, the very narrow region in Fig. 8a, for the $n = 4$ catch, is examined where the resonance state changes to decay. As can be seen, after leaving the $n = 4$ subharmonic resonance, there are three very clear signs of other resonances, namely at the $n = 3, 2, 1$ states. Their positions agree very precisely with the expected values of $a_n = a_1 n^{2/3}$, as shown. None of these resonances have the right conditions to again catch the electron, with one large reason being that during this decay, the orbit is also relaxing from a fairly high eccentricity value of 0.73, and decreasing toward zero. All conditions need to be "right", including ε, A, α, to created a sustained correlation between $\mathbf{F}$ and $\mathbf{v}$. Also, one can see three interesting, very small resonances, that correspond with $\omega_{\frac{n}{m}} = \frac{7}{2}\omega_1$, $\frac{5}{2}\omega_1$, and $\frac{3}{2}\omega_1$ type resonances.

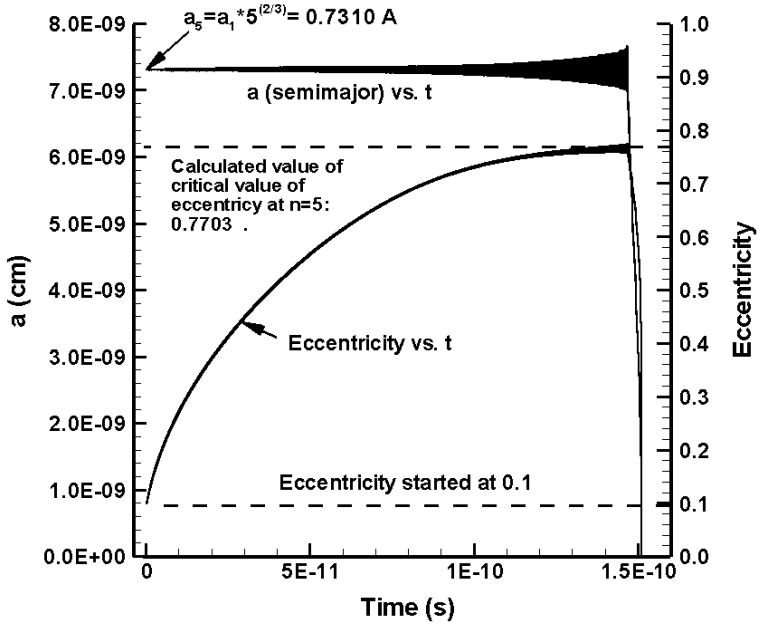

Fig. 8c Here the classical electron was "caught" in an $n = 5$ subharmonic resonance state. $a = 0.25\,\text{Å}$, $a_5 = a_1 5^{2/3} = 0.7310\,\text{Å}$. $A = 75,000$ statvolt/cm, $\alpha = 0$, $\varepsilon_{\text{initial}} = 0.1$, $a_{\text{initial}} = a_5$. The simulation value of $\varepsilon_{\text{crit},5}$ agreed to within the first two digits of the analytically computed value in Table 1 of 0.7703. If we were to blow up the decay region, as in Fig. 8b, now five clear resonant points would be recognizable.

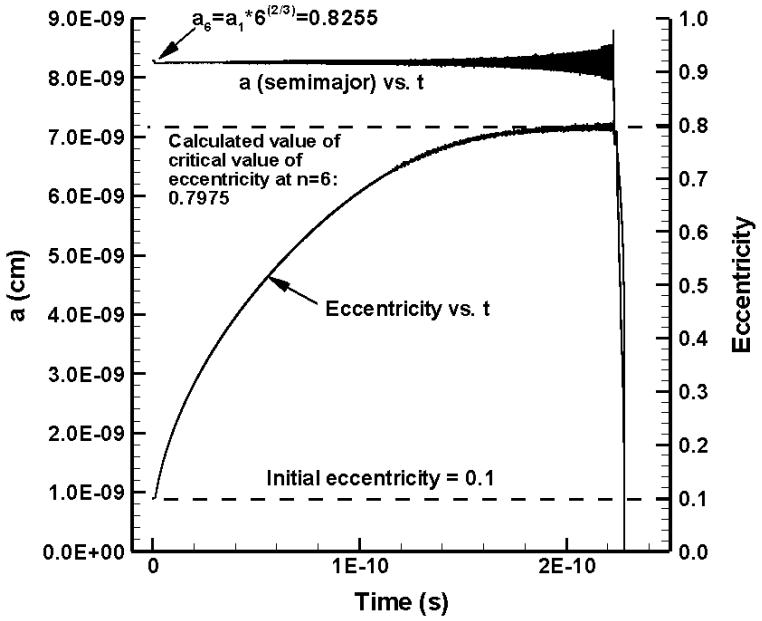

Fig. 8d Here the classical electron was "caught" in an $n = 6$ subharmonic resonance state. $a = 0.25\,\text{Å}$, $a_6 = a_1 6^{2/3} = 0.8255\,\text{Å}$. $A = 75,000$ statvolt/cm, $\alpha = 0$, $\varepsilon_{\text{initial}} = 0.1$. When using $a_{\text{initial}} = a_6 = 0.8255\,\text{Å}$, the electron was not caught, but decayed right through this resonant point, as well as the subsequent $n = 5$, 4, and 3 resonant points, before finally being caught in the $n = 2$ state. However, by changing the a_{initial} ever so slightly, from $a_6 = 0.8255\,\text{Å}$ to $0.83\,\text{Å}$, then the $n = 6$ state was achieved, as shown here. The simulation value of $\varepsilon_{\text{crit},6}$ agreed to within the first 3 to 4 digits of the analytically computed value in Table 1 of 0.7975. If we were to blow up the decay region, as in Fig. 8b, six clear resonant points would be recognizable.

Several investigations were carried out as to why many of the examples here only agree to just two or three digits with the analytic predictions in Table 1, while some examples agree to about four digits. These investigations were carried out for variations in A, α, a_{initial}, and $\varepsilon_{\text{initial}}$. The last two seemed to have the biggest effect in terms of determining $\varepsilon_{\text{crit},n}$ more precisely. In particular, if the electron's orbit is started at a_n, or just slightly above, it turns out that the resonant state will not fully evolve to the situation where L_z relaxes to the condition where $\frac{d}{dt}L_z \to 0$, as in Fig. 6a. This assumption was made in Sec. IV, or rather that $\left\langle \frac{d}{dt}L_z \right\rangle \approx 0$ at the point of decay. This assumption turns out to be not quite true and can lead to a small difference with the predictions of Table 1. Figure 9a illustrates this point for an $n = 2$ situation. Several related examples were carried out, but they all were similar. If a_{initial}.is close to a_n, the resonance point, then the transition from resonance to decay will occur before $\left\langle \frac{d}{dt}L_z \right\rangle$ reaches zero. For the examples checked here, once a_{initial} is larger than a_n by only $0.05\,\text{Å}$ to $0.10\,\text{Å}$, then the approximation of $\left\langle \frac{d}{dt}L_z \right\rangle \approx 0$ at the point of decay is valid.

Otherwise, particularly starting right at a_n, did not provide enough time for the orbital dynamics to evolve to a condition of $\left\langle \frac{d}{dt} L_z \right\rangle \approx 0$ at the point of decay.

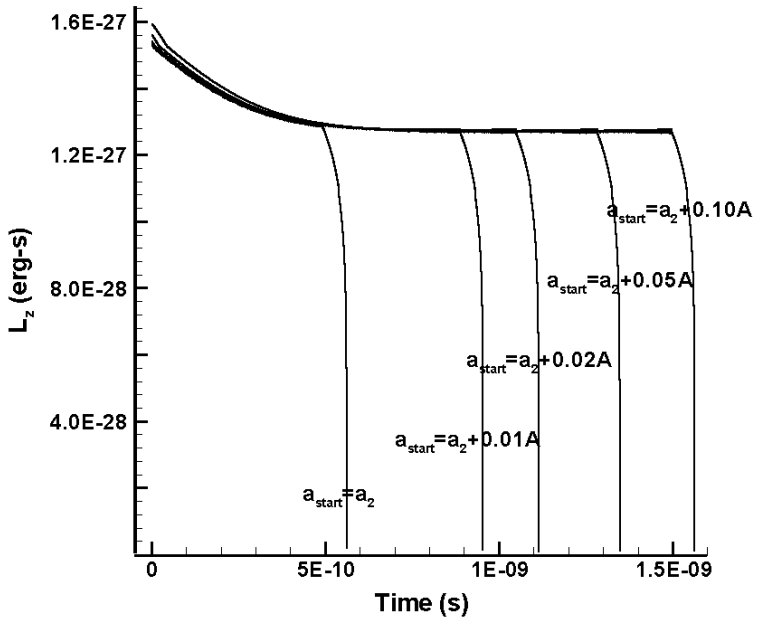

Fig. 9a Five curves are shown here, each a plot of L_z vs. t, but with different starting conditions. In each simulation, $a_1 = 0.7\,\text{Å}$, ω_1 for the CP wave being $\omega_1 = \left(\frac{e^2}{ma_1^3}\right)^{1/2}$, $a_2 = a_1 2^{2/3} \approx 1.1112\,\text{Å}$, $A = 1000$ statvolt/cm, $\varepsilon_{\text{initial}} = 0$, $\alpha = 0$. The first curve on the left has $a_{\text{initial}} = a_2$, so right at the $n = 2$ resonance. The next four curves to the right start at $a_2 + 0.01\,\text{Å}$, $a_2 + 0.02\,\text{Å}$, $a_2 + 0.05\,\text{Å}$, and $a_2 + 0.10\,\text{Å}$, respectively. As can be seen the first curve starting at a_2 does not end with $\left\langle \frac{d}{dt} L_z \right\rangle \approx 0$ at the point of decay, although subsequent curves, starting just slightly above a_2, realize this condition closer and closer.

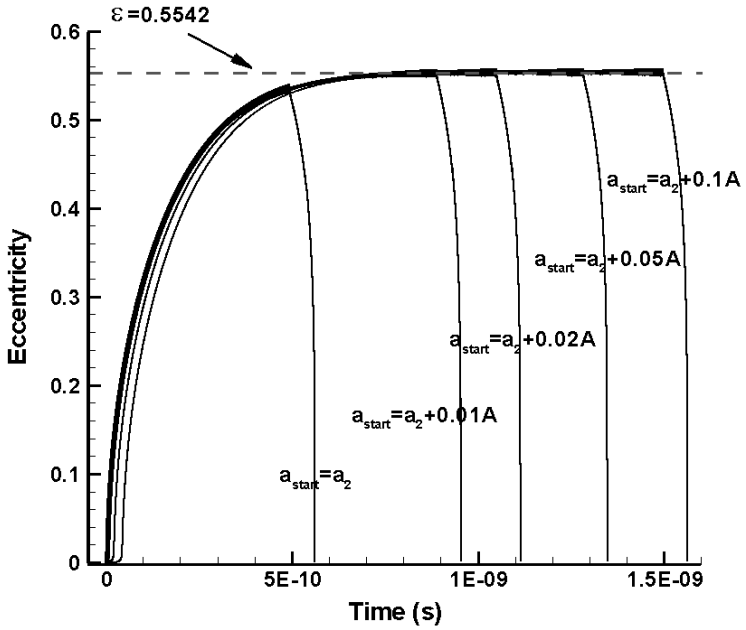

Fig. 9b The same simulation cases as in Fig. 9a are shown here, but now ε vs. t is plotted. The expected $\varepsilon_{\mathrm{crit},2}$ value for $n = 2$ subharmonic resonance as predicted in Table 1 is shown, of $\varepsilon_{\mathrm{crit}} = 0.5542$. As expected by now, the simulation with the classical electron starting at a_2 is a bit off from this predicted value, because of Fig. 9a, which showed that if the electron starts too close to a_2, then $\left\langle \frac{d}{dt} L_z \right\rangle$ will not evolve fully to zero before decay sets in. However, even $a_2 + 0.01\,\text{Å}$ is enough to change this situation quite a bit.

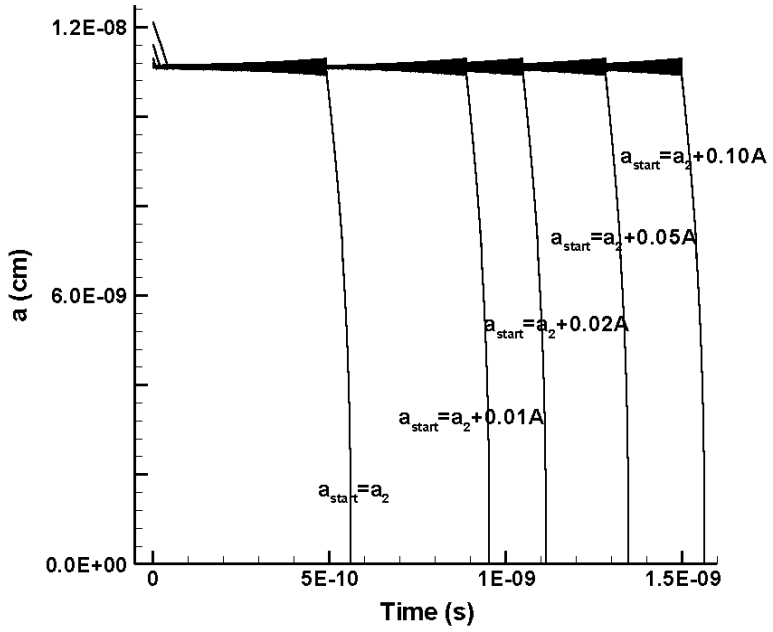

Fig. 9c To put the simulations in Figs. 9 a,b in better perspective, $a\,(t)$ vs. t is shown here for these same five simulation cases. The top lines on the upper left indicate the five starting points in terms of $a_{\rm initial}$. All curves hit resonance and stay there for a while before decaying, with the longer times before decay increasing the larger x is in $a_{\rm initial} = a_2 + x$. Sets of simulations for much larger values of x were carried out as well (0.25 Å, 0.50 Å, 0.75 Å) and this monotonic increase of resonance time with x dies out, as might be expected.

The effect of changing the initial eccentricity is somewhat similar. Both $a_{\rm initial}$ and $\varepsilon_{\rm initial}$ can change the value of $\varepsilon_{{\rm crit},n}$ from the results in Table 1, as well as change whether the classical electron is even "caught" in a long subharmonic resonance or not. For example, if $\varepsilon_{\rm initial}$ is too large, then it is quite possible that no "catch" will be made at all. We have not explored the latter in detail here, but just noted this fact.

6 Concluding remarks

Under the conditions outlined here, where a CP wave of frequency $f_1 = \frac{1}{2\pi}\left(\frac{e^2}{ma_1^3}\right)^{1/2}$ is directed perpendicular to a classical electron's orbit, significant orbital resonances can occur, if the CP wave amplitude A is large enough. The first such resonance behavior that was investigated analytically and via simulation methods for hydrogen and Rydberg atoms, was for the primary resonance situation [2]-[5], when the CP frequency equals the orbital frequency; resonance then occurs at the semimajor axis value of a_1. Reference [1] turned to examining subharmonic resonances that occur at

orbital frequencies $f_n = \frac{1}{n} f_1$ and at semimajor axis values of $a_n = a_1 n^{2/3}$. In many ways, these subharmonic resonances are of even higher interest than the primary ones, as the subharmonic resonances, especially $n = 2, 3$, are able to "catch" a decaying orbit and hold it in resonance without the semimajor axis a decreasing for comparatively long times.

The present article investigated the $n \geq 2$ resonances in more detail, showing some new information, in particular that a remains essentially constant during subharmonic resonance, while the semiminor axis b steadily decreases. When the orbit is initially circular, the eccentricity $\varepsilon = \left[1 - \left(\frac{b}{a}\right)^2\right]^{1/2}$ equals zero, but during subharmonic resonance, ε continues to increase until a critical value, $\varepsilon_{\text{crit},n}$, is reached. In Sec. IV, an analytic derivation was given for these values; see Table 1 and Fig. 7. These are new results, not deduced elsewhere. These values were also calculated via detailed simulation methods for $n = 2, 3, 4, 5, 6$ examples, producing $\varepsilon_{\text{crit},n}$ values that agreed reasonably well with the analytic predictions. As noted, the higher the value of n, the more difficult it became to find values of a_{initial} and $\varepsilon_{\text{initial}}$ to enable the catch and subsequent resonance to be found.

How might these results be utilized? Two possibilities seem of particular interest. First, for a true Rydberg atomic system, where the outer electron is nearly ionized, the quantum energy states of the outer electron are nearly a continuum. The classical physics analysis studied here, should hold extremely well for much of this phenomena. Even though the quantum states are in a near continuum, the classical resonances reported here still hold. Evidently, a classical electron can be held in a classical subharmonic resonance with an incident CP laser beam, for fairly long times. Incidentally, as reported in [1], the larger a_1, the smaller needs to be A to retain the electron in a subharmonic resonance. For example, Fig. 1a-f examined the $n = 2$ case of $a_1 = 0.6\,\text{Å}$ ($a_2 = 0.9524\,\text{Å}$) needing $A = 1000$ statvolt/cm to achieve this resonance. Figures 1g,h examined the $n = 2$ case of $a_1 = 3.0\,\text{Å}$ ($a_2 = 4.7622\,\text{Å}$), but only needing 50 statvolt/cm, considerable less.

By taking advantage of subharmonic resonances, and developing novel schemes for their control, it is possible that new means for reading and writing information to atoms can be realized. Similarly, controlling plasma-like states for etching, display, etc., via strategies not taken before, may be possible. Undoubtedly such controls will likely be of the statistical process control type, since atoms of different initial conditions, even somewhat different, will not all respond the same way. Ensemble variations would need to be taken into account.

The second possible interest here is for more deeply investigating the classical theory of stochastic electrodynamics (SED). This theory considers the interaction of classical charged particles and classical electromagnetic radiation, viewing them both as critically dependent on each other in terms of arriving at any sort of stochastic equilibrium. Relevant background information is contained in [11],[12],[13]. Linear systems such as interacting simple harmonic electric dipole oscillators, are nicely predicted by this theory to be in agreement with quantum electrodynamics. In a few instances, such as uniformly accelerating a system of electric dipole harmonic oscillators through the vacuum [25], [26], [27], or Casimir and van der Waals force calculations at various temperatures [28], [29], [30], [31], SED actually provides a faster and often significantly clearer physical picture for the basis of the calculations.

However, when turning to nonlinear physical systems, agreement with QED has in general not been found. Boyer has been the main person to emphasize that we

should not be seeking agreement with just any nonlinear binding force, but rather only binding forces that actually occur in nature. For the electrodynamic interaction, one of the four recognized physical interactions in nature, and the one that forms the basis for the atomic electron/nucleus construction and arguably the explanation for the atomic properties in the periodic table, the key binding force is of course the Coulombic interaction between nucleus and electrons.

The ground state of hydrogen has been explored by theoretical means in SED, plus more extensively, by detailed simulation efforts [14], [6], [15], [16], [17]. The early simulation work in [6] looked promising for SED's agreement with quantum mechanics, but much more recent work with far more powerful computational power [15], [16], [17], disputes this point. The work in the present article was aimed at providing deeper insight into the simple classical electron dynamics within a Coulombic potential. Some of the early initiative was to gain an understanding of what might give rise to the excited states of hydrogen, thereby helping to go beyond the thermodynamic equilibrium state at absolute zero temperature for the "ground state". Clearly this article does not provide that full insight, but it does raise a number of interesting properties that may be important in the full picture.

Regarding the interesting subharmonic resonance behaviors detailed here, a point made earlier is that the rapidly varying $\mathbf{F} \cdot \mathbf{v}$ power put into the orbit from the CP wave is what dictates the resonance behavior, and also complicates the analytical analysis. The sign of $\mathbf{F} \cdot \mathbf{v}$ varies about n times per orbit in an n subharmonic resonance, with more gradual average changes in the energy (Fig. 1f); the CP wave also alters the orbit, of course, which is what causes an initial circular orbit changing to an elliptical one under resonance conditions.

An interesting insight just from the above observation, is that one key difference with an $n = 1$ resonance versus $n \geq 2$ resonances, is that an $n = 1$ resonance may go for tens or hundreds of orbits before the $\mathbf{F} \cdot \mathbf{v}$ changes in sign, since the CP wave and the orbit only fall out of phase once the orbit grows or shrinks in size (see, for example, Fig. 5 in [2] and Fig. 3 in [4]). In contrast, for $n \geq 2$, this sign change of $\mathbf{F} \cdot \mathbf{v}$ happens about n times for every orbit, giving rise to the stochastic-like behavior in Fig. 1f. Possibly this difference in behavior may result in differences in the ability to "catch and retain" decaying orbits. This conjecture could readily be tested in future work.

The analytic prediction in Sec. IV seems certainly of interest, and reasonably close to the simulations carried out here. However, it should be pointed out that these predictions depend on: (1) the set of approximations that $E = \frac{1}{2}m\mathbf{v}^2 - \frac{e^3}{r} \approx -\frac{e^2}{2a}$, and $L_z = mr^2\dot{\theta} \approx e\,(am)^{1/2}\left(1-\varepsilon^2\right)^{1/2}$, which seem quite sound for the situations examine here; (2) that time averages are taken over the fluctuations in E and L_z, due mainly to the CP plane wave action on the orbit, and (3) that $\left\langle \frac{d}{dt}L_z \right\rangle \approx 0$ when the subharmonic resonance condition changes to one of decay. If the analysis in Sec. IV is to be criticized, it is likely this last point that should be attacked, as it would be better to be able to predict the point of resonance to decay via a more fundamental manner. Otherwise, the predictions seem of interest and reasonably close to simulation prediction.

Some other points that should be made are the following. Clearly the emphasis has been on a single CP wave, as opposed to a linear, or, more generally, an incident electromagnetic radiation with arbitrary elliptical polarization. The reason for focusing on a CP wave is of several fold. First, as first studied in [2] with a CP wave, "ideally"

one can obtain a perfect balance with the radiation reaction, and can then proceed from there to study deviations from this condition. For this reason, some of the initial physical behavior for balance and resonance seems easier to examine with CP waves. Second, any radiation field can be decomposed into CP waves, just as readily as with plane waves. Third, if one does examine, via simulation, just linear or more general elliptically polarized radiation, it turns out that the "signatures" of resonance show up here as well, as in [3]. But, admittedly, the full scope of these other conditions has certainly not be examined here.

In conclusion, the subharmonic resonances for hydrogen and Rydberg atoms provide interesting possibilities for technology applications. In addition, such study provides insight into surprising quasi-stable conditions for classical resonances of an electrodynamic Coulombic atomic system.

Acknowledgements

I thank Dr. Lu Gao for using the code described here to carry out an independent study with me, some time ago, to explore some of the early beginnings of the work reported here. I also thank Professor Timothy Boyer for a recent, enjoyable morning of discussing the results in a first draft of this article and for his ideas on why the $n = 1$ versus $n = 2$ and 3 resonances behave differently in terms of being able to "catch" the classical electron.

References

1. D. Cole and Yi Zou. Subharmonic resonance behavior for the classical hydrogen atomic system. *J. Sci. Comput. (USA)*, 39(1):1 – 27, 2009/04/. hydrogen atomic system;perturbation analysis;nonlinear dynamics;classical charged point particle;nonrelativistic Lorentz-Dirac equation of motion;circular polarization;subharmonic resonance;H₂;.
2. D.C. Cole and Y. Zou. Simulation study of aspects of the classical hydrogen atom interacting with electromagnetic radiation: Circular orbits. *Journal of Scientific Computing*, 20(1):43 – 68, 2004. Circular orbits;Rydberg states;.
3. D. C. Cole and Y. Zou. Simulation study of aspects of the classical hydrogen atom interacting with electromagnetic radiation: Elliptical orbits. *Journal of Scientific Computing*, 20(3):379–404, 2004. Preprint available at http://www.bu.edu/simulation/publications/dcole/publications.html.
4. D. C. Cole and Y. Zou. Perturbation analysis and simulation study of the effects of phase on the classical hydrogen atom interacting with circularly polarized electromagnetic radiation. *Journal of Scientific Computing*, 21(2):145–172, 2004. Preprint available at http://www.bu.edu/simulation/publications/dcole/publications.html.
5. D. C. Cole and Y. Zou. Analysis of orbital decay time for the classical hydrogen atom interacting with circularly polarized electromagnetic radiation. *Phys. Rev. E*, 69(1):16601–1–12, Jan. 2004.
6. D. C. Cole and Y. Zou. Quantum mechanical ground state of hydrogen obtained from classical electrodynamics. *Physics Letters A*, 317(1–2):14–20, Oct. 13, 2003.
7. M. W. Noel, W. M. Griffith, and T. F. Gallagher. Classical subharmonic resonances in microwave ionization of lithium rydberg atoms. *Phys. Rev. A*, 62:063401, 2000.
8. P. M. Koch and K. A. H. van Leeuwen. The importance of resonances in microwave "ionization" of excited hydrogen atoms. *Physics Reports*, 255:289–403, 1995.
9. H. Maeda, D. V. L. Norum, and T. F. Gallagher. Microwave manipulation of an atomic electron in a classical orbit. *Science*, 307:1757–1760, March 18, 2005.
10. J. S. Rigden. *Hydrogen: The Essential Element*. Harvard University Press, Cambridge, Massachusetts, 2002.
11. L. de la Peña and A. M. Cetto. *The Quantum Dice - An Introduction to Stochastic Electrodynamics*. Kluwer Acad. Publishers, Kluwer Dordrecht, 1996.
12. D. C. Cole. Reviewing and extending some recent work on stochastic electrodynamics. In A. Lakhtakia, editor, *Essays on the Formal Aspects of Electromagnetic Theory*, pages 501–532. World Scientific, Singapore, 1993.
13. T. H. Boyer. General connection between random electrodynamics and quantum electrodynamics for free electromagnetic fields and for dipole oscillator systems. *Phys. Rev. D*, 11(4):809–830, 1975.
14. T. H. Boyer. Random electrodynamics: The theory of classical electrodynamics with classical electromagnetic zero–point radiation. *Phys. Rev. D*, 11(4):790–808, 1975.
15. Theo M Nieuwenhuizen and Matthew T P Liska. Simulation of the hydrogen ground state in stochastic electrodynamics. *Physica Scripta*, 2015(T165):014006, 2015.
16. Theodorus M. Nieuwenhuizen and Matthew T. P. Liska. Simulation of the hydrogen ground state in stochastic electrodynamics-2: Inclusion of relativistic corrections. *Foundations of Physics*, 45(10):1190–1202, 2015.
17. Theodorus M. Nieuwenhuizen. On the stability of classical orbits of the hydrogen ground state in stochastic electrodynamics. *Entropy*, 18(4):135, 2016.
18. C. Teitelboim, D. Villarroel, and Ch. G. van Weert. Classical electrodynamics of retarded fields and point particles. *Riv. del Nuovo Cimento*, 3(9):1–64, 1980.
19. John David Jackson. *Classical Electrodynamics*. John Wiley & Sons, 2nd edition, 1975.
20. G. N. Plass. Classical electrodynamic equations of motion with radiative reaction. *Rev. Mod. Phys.*, 33(1):37–62, 1961.
21. W. H. Press, S. A. Teukolsky, W. T. Vetterling, and B. P. Flannery. *Numerical Recipes in C: The Art of Scientific Computing*. Cambridge University Press, New York, second edition, 1992.
22. H. Goldstein. *Classical Mechanics*. Addison–Wesley, Reading, MA, second edition, 1981.
23. T. L. Chow. *Classical Mechanics*. John Wiley & Sons, Inc., New York, 1995.
24. R. A. Becker. *Introduction to Theoretical Mechanics*. McGraw-Hill, New York, 1954.
25. T. H. Boyer. Thermal effects of acceleration through random classical radiation. *Phys. Rev. D*, 21(8):2137–2148, 1980.

26. T. H. Boyer. Thermal effects of acceleration for a classical dipole oscillator in classical electromagnetic zero-point radiation. *Phys. Rev. D*, 29(6):1089–1095, 1984.
27. D. C. Cole. Thermal effects of acceleration for a spatially extended electromagnetic system in classical electromagnetic zero-point radiation: Transversely positioned classical oscillators. *Phys. Rev. D*, 35:562–583, 1987.
28. T. H. Boyer. Temperature dependence of van der waals forces in classical electrodynamics with classical electromagnetic zero–point radiation. *Phys. Rev. A*, 11:1650–1663, 1975.
29. D. C. Cole. Derivation of the classical electromagnetic zero–point radiation spectrum via a classical thermodynamic operation involving van der waals forces. *Phys. Rev. A*, 42:1847–1862, 1990.
30. D. C. Cole. Entropy and other thermodynamic properties of classical electromagnetic thermal radiation. *Phys. Rev. A*, 42:7006–7024, 1990.
31. D. C. Cole. Reinvestigation of the thermodynamics of blackbody radiation via classical physics. *Phys. Rev. A*, 45:8471–8489, 1992.